The brain of a nocturnal migratory insect, the Australian Bogong moth

Andrea Adden[1], Sara Wibrand[1], Keram Pfeiffer[2], Eric Warrant[1], Stanley Heinze[1]

[1] Lund Vision Group, Lund University, Sweden
[2] University of Würzburg, Germany

Correspondence: andrea.adden@biol.lu.se

Abstract
Every year, millions of Australian Bogong moths (*Agrotis infusa*) complete an astonishing journey: in spring, they migrate from their breeding grounds to the alpine regions of the Snowy Mountains, where they endure the hot summer in the cool climate of alpine caves. In autumn, the moths return to their breeding grounds, where they mate, lay eggs and die. Each journey can be over 1000 km long and each moth generation completes the entire roundtrip. Without being able to learn any aspect of this journey from experienced individuals, these moths can use visual cues in combination with the geomagnetic field to guide their flight. How these cues are processed and integrated in the brain to drive migratory behaviour is as yet unknown. Equally unanswered is the question of how these insects identify their targets, i.e. specific alpine caves used as aestivation sites over many generations. To generate an access point for functional studies aiming at understanding the neural basis of these insect's nocturnal migrations, we provide a detailed description of the Bogong moth's brain. Based on immunohistochemical stainings against synapsin and serotonin (5HT), we describe the overall layout as well as the fine structure of all major neuropils, including all regions that have previously been implicated in compass-based navigation. The resulting average brain atlas consists of 3D reconstructions of 25 separate neuropils, comprising the most detailed account of a moth brain to date. Our results show that the Bogong moth brain follows the typical lepidopteran ground pattern, with no major specializations that can be attributed to their spectacular migratory lifestyle. Comparison to the brain of the migratory Monarch butterfly revealed nocturnal versus diurnal lifestyle and phylogenetic identity as the dominant parameters determining large-scale neuroarchitecture. These findings suggest that migratory behaviour does not require widespread modifications of brain structure, but might be achievable via small adjustments of neural circuitry in key brain areas. Locating these subtle changes will be a challenging task for the future, for which our study provides an essential anatomical framework.

Keywords
Insect brain, lepidoptera, noctuid, central complex, mushroom body

Abbreviations

PC	Unstructured protocerebrum	LO	Lobula
OL	Optic lobe	LOP	Lobula plate
ME	Medulla	LA	Lamina

AME	Accessory medulla	EB	Ellipsoid body
AL	Antennal lobe	PB	Protocerebral bridge
MB	Mushroom body	NO	Nodulus
CA	Calyx	AOTU	Anterior optic tubercle
PED	Pedunculus	UU	Upper unit
ACA	Accessory calyx	LU	Lower unit
SP	Spur	NU	Nodular unit
dL	Dorsal lobelet	ONP	Ocellar neuropil
vL	Ventral lobelet	POTU	Posterior optic tubercle
LX	Lateral complex	POC	Posterior optic commissure
LAL	Lateral accessory lobe	IT	Isthmus tract
BU	Bulb	iLALT	Inter-LAL tract
GA	Gall	SOG	Suboesophageal ganglion
CX	Central complex	AOT	Anterior optic tract
FB	Fan-shaped body		

Introduction

How do behaviours arise from neural signalling? This is one of the central questions in neuroscience. From the sensory input that elicits a behaviour, via further processing and integration of other information that adjusts the behaviour, to the motor circuits that execute the behaviour – the neural processing is complex and as yet we only understand small pieces of this multi-level puzzle. To delve deeper into this question, we need an animal model that shows a robust behaviour and whose brain is accessible enough to allow for detailed physiological and genetic studies. In terms of accessibility, insects have long been reliable model organisms (Clarac & Pearlstein, 2007), as they have comparatively small brains that control a broad and remarkably complex behavioural repertoire. In this study, we focus on one particular insect: the Bogong moth *Agrotis infusa*.

The Bogong moth is one of the most iconic Australian insect species, well known for its spectacular long-distance migrations, carried out during the night (E. Warrant et al., 2016). Each spring, Bogong moths eclose from their pupae in their breeding grounds in Southern Queensland and western New South Wales and Victoria (Australia). After hatching, the moths in each breeding region embark on a 1000 km long journey to the Australian Alps, the country's highest peaks, where they settle down in specific, high-altitude caves (Common, 1954; Warrant et al., 2016). There they enter a state of dormancy ("aestivation") for several months, with the cool alpine climate allowing them to survive the hot summer season. In early autumn, the moths migrate back to their respective breeding grounds, where they mate, lay eggs and die. These seasonal migrations are similar to the migrations of the day-active Monarch butterfly in North America (Reppert, Guerra, & Merlin, 2016). Unlike this species, which completes the migratory cycle over several generations, every Bogong moth completes the entire return journey, from the breeding grounds to the mountain caves and back to the breeding grounds (Common, 1954). In the breeding grounds, the offspring of the

returned migrants hatch in spring and begin the cycle anew.

Crucially, if a moth loses the migratory heading during its long-distance flight, it will miss either its aestivation site (spring) or the breeding grounds (autumn). In either case it will likely not survive the journey and thus fail to reproduce. Therefore, as in all migratory animals, significant selective pressure maintains the stability and accuracy of the migratory behaviour in the Bogong moth. Based on behavioural data, migratory Bogong moths can use the geomagnetic field in combination with visual cues to control their flight heading (Dreyer et al., 2018). Furthermore, it is likely that the moths use olfactory cues to locate their specific aestivation caves in the mountains at the end of their long-range flight (Warrant et al., 2016). The moths need to solve two consecutive problems: first, they must maintain a stable course across many hundreds of kilometres of unfamiliar landscape, and second, they must abort this long-range flight and search for a suitable aestivation site. Both processes cannot rely on learning, as each moth only lives through one migratory cycle. It is currently unknown how the different sensory modalities are integrated with each other, and combined with inherited information, to produce a consistent behaviour. During migration, the moth's brain carefully controls a complex series of navigational decisions, which must be based on hardwired neural circuits. Investigating the relationship between structure and function in the Bogong moth brain therefore provides a unique access point for understanding the neural basis of long-distance, nocturnal migration in Bogong moths. This includes the neural encoding of heading estimates based on multiple sensory cues, the representation of an inherited target direction, the inherited identification of target caves, the season-dependent switch between target headings, mechanisms of course control, and the motivational control of migratory versus non-migratory behaviour. As the overall behavioural pattern is both highly reproducible as well as complex, a thorough understanding of its neural underpinnings will generate a simple model system that might also shed light on the sensory-motor transformations underlying other complex behaviours, including those in larger brains.

Before we can begin to explore the neural implementation of migratory behaviour in the Bogong moth brain, it is imperative that we understand the overall anatomy of the brain. This will generate a morphological framework into which we can embed all future functional work. In this study, we therefore present the detailed outline of the Bogong moth brain.

To this end, we have carried out a combination of immunohistochemical stainings and 3D reconstructions of whole-mount and sectioned Bogong moth brains to produce a comprehensive description of all major regions in the brain of this species, similar to those published for example for the Monarch butterfly (Heinze & Reppert, 2012), the dung beetle (Immonen, Dacke, Heinze, & el Jundi, 2017), the fruit fly (Ito et al., 2014; Jenett et al., 2012), and the locust (von Hadeln, Althaus, Häger, & Homberg, 2018). To account for inter-individual variation, we additionally produced a standardised brain atlas, which robustly describes the average shape of the male Bogong moth brain. Taken together, our detailed descriptions of all neuropils and the overall standard atlas lay the groundwork for future anatomical, physiological and genetic studies of the neural basis of Bogong moth migration and navigation.

Materials and Methods

Animals

Aestivating Bogong moths (*Agrotis infusa*) were collected in a cave on South Ramshead (Kosciuzko National Park, New South Wales, Australia) and transported to Sweden in cooled plastic containers. In the lab, the aestivating moths were kept in a temperature-controlled incubator (I-30 VL, Percival/CLF Plant Climatics, Wertingen, Germany) in cave-like conditions (16 hours dim light at 10 °C, 8 hours dark at 6 °C). The moths had free access to food solution (2% sugar, 2% honey, 0.2% ascorbic acid in water).

In the experiments described below, female and male moths were used. At the time of the experiment, Bogong moths were several months old, as the adults survive up to 8-9 months in the wild if they estivate during the summer (Warrant et al., 2016).

Antibodies

In the following histology protocols, we used antibodies against synapsin and serotonin (5-HT). Both antibodies are described in detail in Table 1. The anti-synapsin antibody was kindly provided by Dr. E. Buchner (Würzburg University, Germany; Cat# SYNORF1 (*Drosophila* synapsin I isoform), RRID: AB_2315426; (Klagges et al., 1996)). For stainings against serotonin we used the 5-HT rabbit antibody from Immunostar (Hudson, WI, USA; Cat# 20080, Lot# 051007). The secondary antibodies were GAM-Cy5 (goat anti mouse conjugated to Cy5; Jackson Immunoresearch Laboratories Inc., West Grove, PA, USA; Cat# 115-175-146, Lot# 108262) and GAR-488 (goat anti rabbit conjugated to Alexa Fluor 488; Invitrogen, Eugene, OR, USA; Cat# A-11008, Lot# 57099A). Normal goat serum (NGS; Jackson Immunoresearch, West Grove, PA, USA; Cat# 005-000-121, Lot# 126560) was used for blocking non-specific antibody binding sites.

Immunohistochemistry protocols

The whole-mount staining protocol was adapted from the protocols described in Ott (2008), Heinze and Reppert (2012) and Stöckl and Heinze (2015). Moth heads were mounted in a wax-filled petri dish and dissected to expose the brain. Fresh zinc-formaldehyde fixative (18.4 mM $ZnCl_2$, 135 mM NaCl, 35 mM sucrose, 1% PFA; (Ott, 2008)) was immediately applied to the brain, which was then dissected out of the head capsule, cleaned of trachea and fat body, and the retina was removed. Brains were left to fix for 20 hours at 4°C and were then washed 8x20 minutes in HEPES-buffered saline (HBS: 150 mM NaCl, 5 mM KCl, 5 mM $CaCl_2$, 25 mM sucrose, 10 mM HEPES; (Ott, 2008)). Brains were bleached in 10% H_2O_2 in Tris-buffered saline (Tris-HCl) for 8 hours (Stöckl & Heinze, 2015). For some preparations, the bleaching step was omitted. Subsequently, brains were washed in Tris-HCl (3x10 minutes), permeabilized in a fresh mixture of dimethyl sulfoxide (DMSO) and methanol (20:80, 70 minutes) and washed again in Tris-HCl (3x10 minutes). After pre-incubating the brains in 5% normal goat serum (NGS) in 0.01 M phosphate-buffered saline (PBS) with 0.3% TritonX-100 (PBS-Tx) over night at 4°C, brains were transferred to the primary antibody solution (anti-synapsin 1:25, 1% NGS in PBS-Tx) and left to incubate at 4°C for 6 days. Brains were washed 8x20 minutes

TABLE 1 Primary antibodies.

Antigen	Immunogen	Manufacturer, species, type, catalog number	Dilution
Synapsin	Fusion protein of glutathione-S-transferase and the *Drosophila* SYN1 protein	Developed by and obtained from G. Buchner (Würzburg University, Germany), mouse, monoclonal, CAT# SYNORF1, RRID: AB_2315426	1:25 (wholemount), 1:50 (section)
Serotonin	Serotonin coupled to bovine serum albumin (BSA) with paraformaldehyde	Immunostar (Hudson, WI, USA), rabbit, polyclonal, CAT# 20080, Lot# 051007	1:1000

in PBS-Tx before being transferred to the secondary antibody solution (1:300 GAM-Cy5, 1% NGS in PBS-Tx) and left to incubate at 4°C for 5 days. Before mounting, brains were washed in PBS-Tx (6x15 minutes) and PBS (2x15 minutes) and dehydrated in an increasing ethanol series (50%, 70%, 90%, 96%, 2x100%, 15 minutes each). For clearing, brains were transferred to a fresh mixture of ethanol and methylsalicylate (1:1) and the ethanol was allowed to evaporate. After 15 minutes, the mixture was replaced by pure methylsalicylate, in which the brains were left to clear for up to 75 minutes. Finally, the brains were embedded in Permount (Electron Microscopy Science, Hartfield, PA, USA) between two coverslips, using plastic spacers (Zweckform No. 3510, Germany) to prevent squeezing.

For brain sections, we used a protocol adapted from the sectioning protocol described in (Heinze & Reppert, 2012). Brains were dissected in moth ringer solution (150 mM NaCl, 3 mM KCl, 10 mM TES, 25 mM sucrose, 3 mM $CaCl_2$; based on (King, Christensen, & Hildebrand, 2000)), immediately transferred to Zamboni's fixative (4% PFA, 7.5% picric acid in 0.1 M phosphate buffer) and left to fix over night at 4°C. The brains were then washed in PBS (3x10 minutes), embedded in albumin-gelatin (4.8% gelatin and 12% ovalbumin in demineralized water) and post-fixed in 4% formaldehyde solution (in 0.1 M PBS). A vibratome (Leica VT1000 S, Leica Biosystems, Nussloch, Germany) was used to cut the brains into 40 μm thick sections, which were then washed in 0.1 M PBS and pre-incubated in 5% NGS in PBS-Tx (1 hour) before being transferred to the primary antibody solution (1:50 anti-synapsin, 1:1000 anti-5HT, 1% NGS in PBS-Tx, incubate over night at room temperature). The sections were rinsed in PBS-Tx (8x10 minutes) and transferred to the secondary antibody solution (1:300 GAM-Cy5, 1:300 GAR-488, 1% NGS in PBS-Tx, incubated over night at room temperature). Before mounting, the sections were washed in PBS-Tx (3x10 minutes) and then mounted on chromalaun/gelatine-coated glass slides and left to dry for at least 5 hours. Once dry, the sections were dehydrated in an increasing ethanol series (demineralized water (5 minutes); 50%, 70%, 90%, 96%, 2x100% ethanol (3 minutes each)), cleared in

xylene (2x5 minutes) and embedded in Entellan (EMS, Hatfield, PA).

For high resolution image stacks of immunolabeled brains, thick sections were prepared. In the current study these were obtained from neurobiotin injected brains that had previously been imaged at low resolution. These brains were incubated in xylene for several hours to remove the Permount mounting medium. Then the brains were rehydrated in a series of decreasing ethanol concentrations (15 minutes each, reverse order from above). After washing the brains in 0.01 M PBS (3x15 minutes), they were embedded in albumin-gelatin and post-fixed as described above. Sections of 140 μm thickness were obtained with a vibrating blade microtome. Immunohistochemistry against synapsin and 5TH was performed in a similar manner to whole-mount preparations. Free floating sections were rinsed in PBS (3x15 minutes), pre-incubated with 5% NGS in PBT (5 hours) and subjected to primary antibody incubation (2-3 days at 4˚C; concentrations as above). After rinsing with PBT (6x15 minutes), the secondary antibody incubation was performed (1-2 days at 4°C; concentrations as above). The sections were then rinsed (4x15 minutes PBT and 2x15 minutes PBS), before being dehydrated in an increasing series of ethanol concentrations (10 minutes each step, concentrations as above). Finally, the sections were cleared in Methylsalicylate and mounted in Permount between two coverslips, separated by spacers.

Classic histology and dye injections

For Azur II-methylene blue staining, brains were fixed over night at 4˚C (in 2% paraformaldehyde, 2.5% glutaraldehyde, 2mM $CaCl_2$ in 0.1M sodium cacodylic buffer). This was followed by rinsing in 0.1M sodium cacodylic buffer, dehydration in an increasing ethanol series (70% 2x10 minutes, 96% 2x10 minutes, 100% 2x15 minutes) and infiltration in an acetone/Epon plastic series (acetone 2x20 minutes, 2:1 acetone/Epon 1 hour, 1:1 acetone/Epon over night, pure Epon 6 hours). The samples were embedded in fresh Epon and polymerised at 60°C for 48 hours. Samples were then sectioned in 1 μm sections on a Leica Ultracut UCT ultramicrotome using a diamond histoknife. The sections were mounted on chromalum-gelatine coated microscope slides and stained with one drop of Azur II-methylene blue.

Single neurons were injected with 4% neurobiotin solution (in 1M KCl) using a sharp micropipette during intracellular recordings (for details see e.g. (Stone et al., 2017)). Mass dye injections were performed with glass micropipettes whose tips had been broken off with a pair of tweezers. The tips of the resulting blunt micropipettes were coated in petroleum jelly and dipped into neurobiotin powder. Injections were then carried out by manually inserting the micropipette into the region of interest (antennal lobe or optic lobe). For both types of injections, the brains were dissected out of the head capsule in moth ringer solution and subsequently fixed in neurobiotin fixative (4% paraformaldehyde, 0.25% glutaraldehyde, 2% saturated picric acid in 0.1M phosphate buffer) over night at 4°C. Brains were then washed 4x15 minutes in 0.1M PBS and left to incubate in streptavidin-Cy3 or streptavidin-Cy5 (1:1000 in PBT) at 4°C for three days. After washing 6x20 minutes in PBT and 2x20 minutes in PBS, the protocol then followed the wholemount staining protocol for dehydration, clearing and mounting.

Confocal imaging

Images were taken with a confocal laser scanning microscope (LSM 510 Meta, Zeiss,

Jena, Germany, or Leica TCS SP8, Leica Microsystems, Wetzlar, Germany).

For 3D reconstructions of anti-synapsin labelled preparations, whole-mount brains were imaged with the Zeiss LSM 510 Meta, using the 633nm HeNe laser and a 10x objective (C-Apochromat 10x/0.45W, Zeiss) or, for high resolution scans, using a 25x objective (LD LCI Plan-Apochromat 25x/0.8 DIC Imm Corr, Zeiss). Scans from anterior and posterior were later aligned and merged in the 3D reconstruction software Amira 5.3.3 (FEI, Hillsboro, OR, USA). Scans of whole-mount preparations were acquired as stacks of 1 μm thick optical sections at 1024x1024 resolution. The detector range was set to 650-700 nm and the pinhole was set to 1 airy unit. Detector gain and offset as well as laser power were adjusted for each section in order to optimally expose the image.

High-resolution scans of neurobiotin-labelled neurons were obtained with a 63x glycerol immersion objective (HC PL APO CS2 63x/1.30 GLYC) on a Leica TCS SP8 microscope. Sectioned brains were scanned using the 25x objective or, for detailed images, using the 40x objective (Plan-Neofluar 40x/1.3 Oil DIC, Zeiss), using the 633nm HeNe and the 488nm Ar lasers. Using the hybrid detector (HyD™) of the Leica TCS SP8 microscope, high resolution scans of sections were obtained with the 20x objective (HC PL APO 20x/0.75 IMM CORR CS2) or the 63x objective (HC PL APO 63x/1.40 Oil CS2). Section images were acquired as stacks of 1μm thick optical sections at 1024x1024 resolution. The detector range was set to 650-700 nm for Cy5 and 500-600 nm for Alexa488 labelled sections. The two channels were always scanned sequentially. The pinhole was set to 1 airy unit.

Scans were aligned and merged using the stitching tool in the ImageJ implementation FIJI (general public license, downloadable from http://fiji.sc (Schindelin et al., 2012); stitching algorithm based on (Preibisch, Saalfeld, & Tomancak, 2009)). Images were generally optimized for brightness and contrast. Some images were denoised using the 3D hybrid median filter algorithm implemented in FIJI (https://imagej.nih.gov/ij/plugins/hybrid3dmedian.html). All confocal images shown in this paper are single optical slices (unless stated otherwise). The terms dorsal, ventral, anterior and posterior refer to the body axis of the animal.

Three-dimensional reconstructions

The neuropil reconstructions shown in this paper were done in the 3D reconstruction software Amira 5.3.3, and are based on anti-synapsin labelled whole-mount brains. Image stacks were down-sampled to a voxel size of 2x2x2 μm. Each voxel was then assigned to an individual brain area using the segmentation editor of Amira, and the full structure of reconstructed neuropils was interpolated using the "wrap" function. Neuropil volumes were extracted using Amira's "MaterialStatistics" function. We generated a polygonal surface model to visualise the neuropils.

Standardisation

To generate the standard confocal image stack, we used the computational morphometry toolkit (CMTK 3.2.3) and the iterative shape averaging (ISA) protocol to create an average image stack from 10 individual image stacks (Rohlfing, Brandt, Maurer, & Menzel, 2001). Calculations were carried out at the University of Marburg on the high-performance Linux cluster MaRC2, using a 64 core (4x AMD Opteron 6276 Interlagos) node with 4 GB of RAM per core.

Of the 10 individual brains, we chose the one that was the most representative of the population in terms of volume and shape as the reference for standardisation. All other brains were first affinely registered to the reference brain, to compensate for differences in size, position and rotation. After affine registration, an average image stack was computed from all 10 brains, which served as a template for the subsequent elastic registration processes. Elastic registration applies local transformations to each brain, thereby optimising the similarity between images. The resulting images were used to compute a new average image stack, which was the template for a second elastic registration. This was repeated five times. The final average image stack was accepted as the standard image stack, and the registration parameters that were applied to each brain were then applied to the corresponding neuropil reconstructions. Finally, we used the shape-based averaging method to obtain the standard surface reconstruction (Rohlfing & Maurer, 2007). A detailed description of the method can be found in (de Vries et al., 2017). Since the lamina was only intact in three specimens, the average lamina was generated separately and later added to the standard brain. Furthermore, the unstructured protocerebrum shown in this paper was reconstructed after standardisation from the standard confocal image stack. During standardisation of the neuropil surfaces, the anterior and posterior parts of the right Y-tract became separated, which was fixed manually after standardisation by re-reconstructing this part of the neuropil from the average image stack.

Data accessibility

The reconstructed male standard brain and the individual female brains, as well as the standard confocal image stack, are freely available on insectbraindb.org, species handle https://hdl.handle.net/20.500.12158/SIN-0000002.1.

Results

The aim of the anatomical data presented in this study is to provide a reliable framework for future anatomical and functional work in the Bogong moth. Beyond the goal of describing each neuropil, our data also allows the direct comparison of anatomical data from many individual brains, for instance data resulting from intracellular recordings combined with dye injections. To this end we have generated a standardised atlas of the male Bogong moth brain (Figure 1). Data from individual brains can be reliably registered into this standard brain, as inter-individual differences in size and shape have been averaged. This average brain additionally provides a reference data-set of representative neuropil volumes, that is, a basis for volumetric comparisons with other insects (Figure 2). The male standard brain is the average of 10 individual brains, generated by the iterative shape averaging (ISA) protocol, using the CMTK toolkit (Rohlfing et al., 2001). As the lamina of the optic lobe was only intact in three individuals, we averaged those separately and combined the resulting average with the standard brain. The undefined neuropils of the central brain were reconstructed as a surface model based on the average image stack rather than in each individual brain.

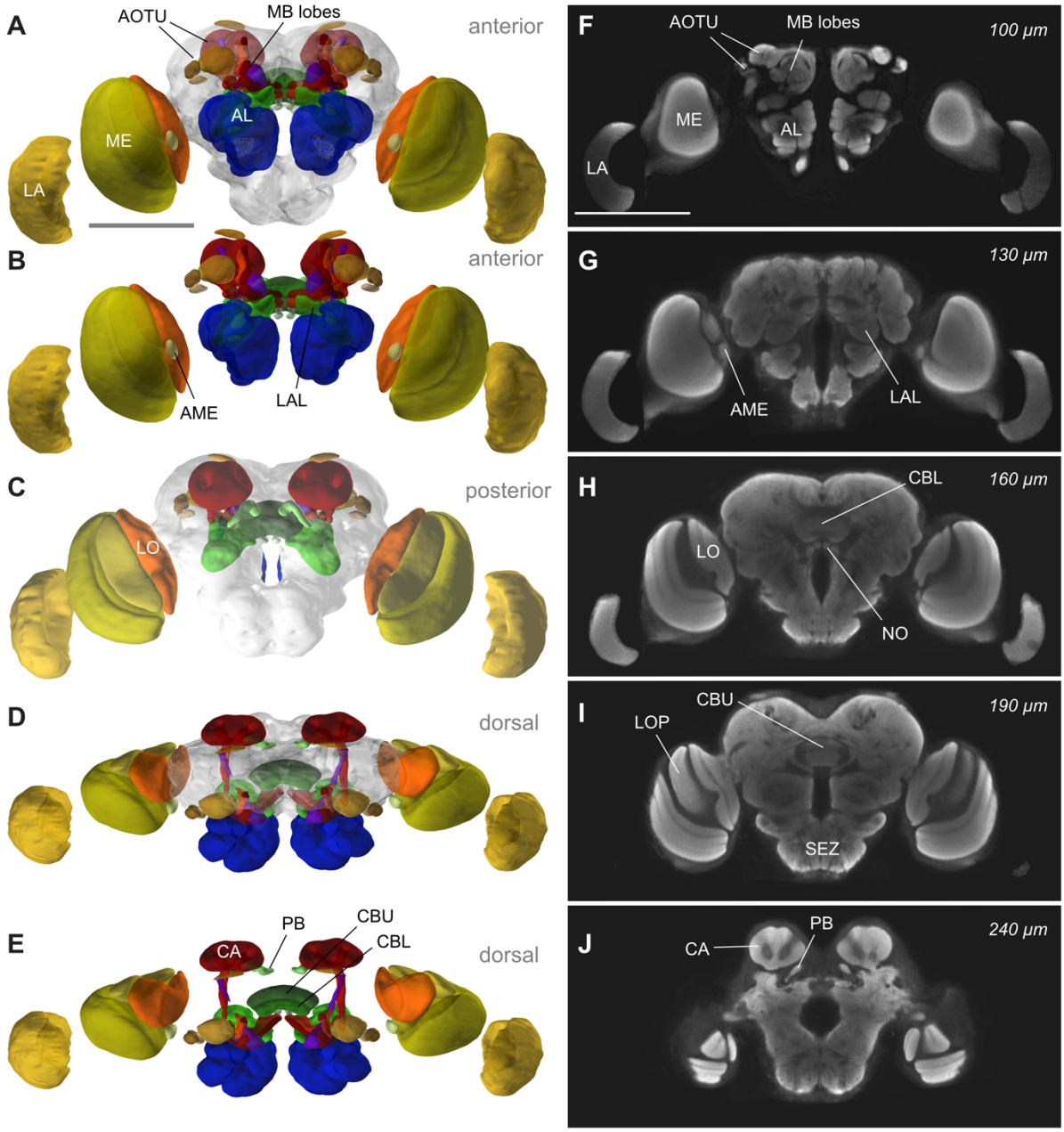

FIGURE 1 The Bogong moth standard brain. (A) Anterior view of the male standard brain reconstruction. Here and in all following figures, the colour code is as follows: yellow – visual input areas (optic lobes and ocellar neuropils), brown – anterior optic tubercle, red – mushroom bodies, green – central complex and lateral complex, blue – antennal lobes, grey – unstructured protocerebrum. (B) Anterior view without the unstructured protocerebrum, to show the arrangement of neuropils within the central brain. (C) Posterior view of the brain, with the lobula plate, ocellar neuropils, mushroom body calyces and protocerebral bridge visible. (D, E) Dorsal view of the brain with and without the unstructured protocerebrum. (F-J) Optical sections through the standard brain progressing from anterior to posterior. Note that the lamina of the standard brain was calculated separately from three available specimens and added to the standard brain later. Scale bars = 500 μm.

In total, we have reconstructed 25 individual neuropils (23 paired and 2 unpaired). These include five compartments of the optic lobes (OL), the antennal lobes (AL), three subunits of the anterior optic tubercle (AOTU), eight neuropils of the mushroom bodies (MB), four compartments of the central complex (CX), three compartments of the lateral complex (LX),

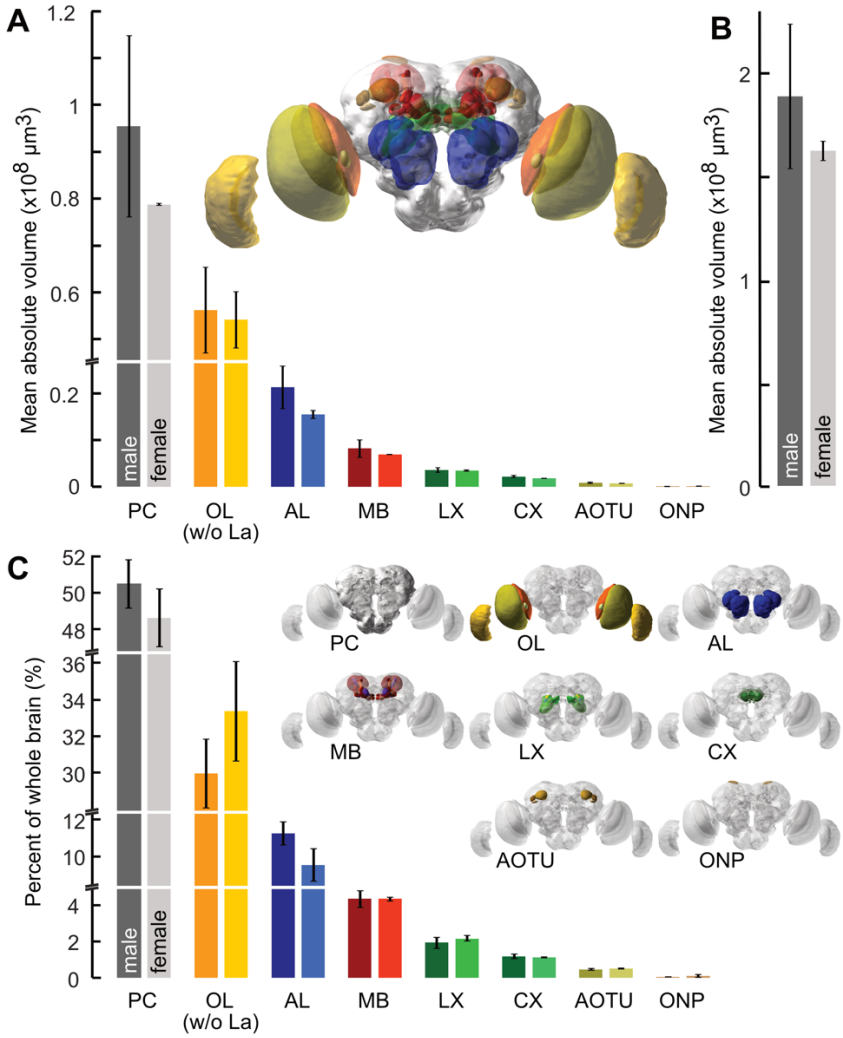

FIGURE 2 Volumetric analysis of the Bogong moth brain. (A) Mean absolute volumes of the neuropils within the male and female Bogong moth brain. (B) Mean absolute volumes of the complete male and female brain, excluding the lamina. (C) Comparison of the volume contributions of each neuropil to the whole brain, for 6 male and 2 female Bogong moths. Note that the optic lobes exclude the lamina, which was only intact in four samples (three males and one female).

and the combined mass of the remaining undefined neuropils of the central brain.

Complete volumetric analysis was carried out in six out of the ten male brains used for shape averaging and in two additional female individuals. The male Bogong moth brain was found to be slightly larger than the female, with overall volumes of 0.188 ± 0.035 mm^3 (males) and 0.162 ± 0.005 mm^3 (females; Table 2, Figure 2B). When normalizing to overall brain volume, we found no gross differences between the male and female brain, with the notable exception of the antennal lobe, which displayed a male-specific macroglomerular complex (MGC), which is a pronounced sexual dimorphism typical for moths (B. G. Berg, Almaas, Bjaalie, & Mustaparta, 1998; A. Stöckl et al., 2016). In relative terms, the undefined protocerebrum makes up the largest part of the brain, accounting for ca. 50% of the total volume (Table 3, Figure 2C). The second most voluminous neuropil group is the optic lobe, occupying about one third of the total brain volume. Half of the remaining 20% of brain volume is occupied by the antennal lobes. Finally, all other brain regions combined (mushroom body, lateral complex, CX, AOTU, ocellar neuropils) account for ca. 10% of total brain volume. The inter-individual variation within the population of our wild-caught Bogong moth sample was comparably high. Across the six male brains, neuropil volumes varied between 13% and 56% around the mean (Table 3), with the

smallest neuropils having the largest relative variability.

In the following, all brain regions will be described in detail, starting with the primary sensory areas and moving towards more central, higher-order regions.

Optic neuropils

The Bogong moth possesses two types of eyes: firstly, the large superposition compound eyes on either side of the head, and secondly, two ocelli, which are small lens eyes located just dorsally of the compound eyes. The ocelli are connected to the brain via the thin ocellar nerve, which enters the brain dorsally near the mushroom body calyx. The axons of the ocellar photoreceptors terminate in the ocellar neuropil (ONP), an elongated, irregularly shaped brain area on either side of the midline (Figure 3A, B).

Underlying the retinae of the compound eyes, the Bogong moth optic lobes contain four highly structured neuropils: three large neuropils stacked from distal to proximal (lamina, medulla, lobula), and the posteriorly located lobula plate. Finally, the

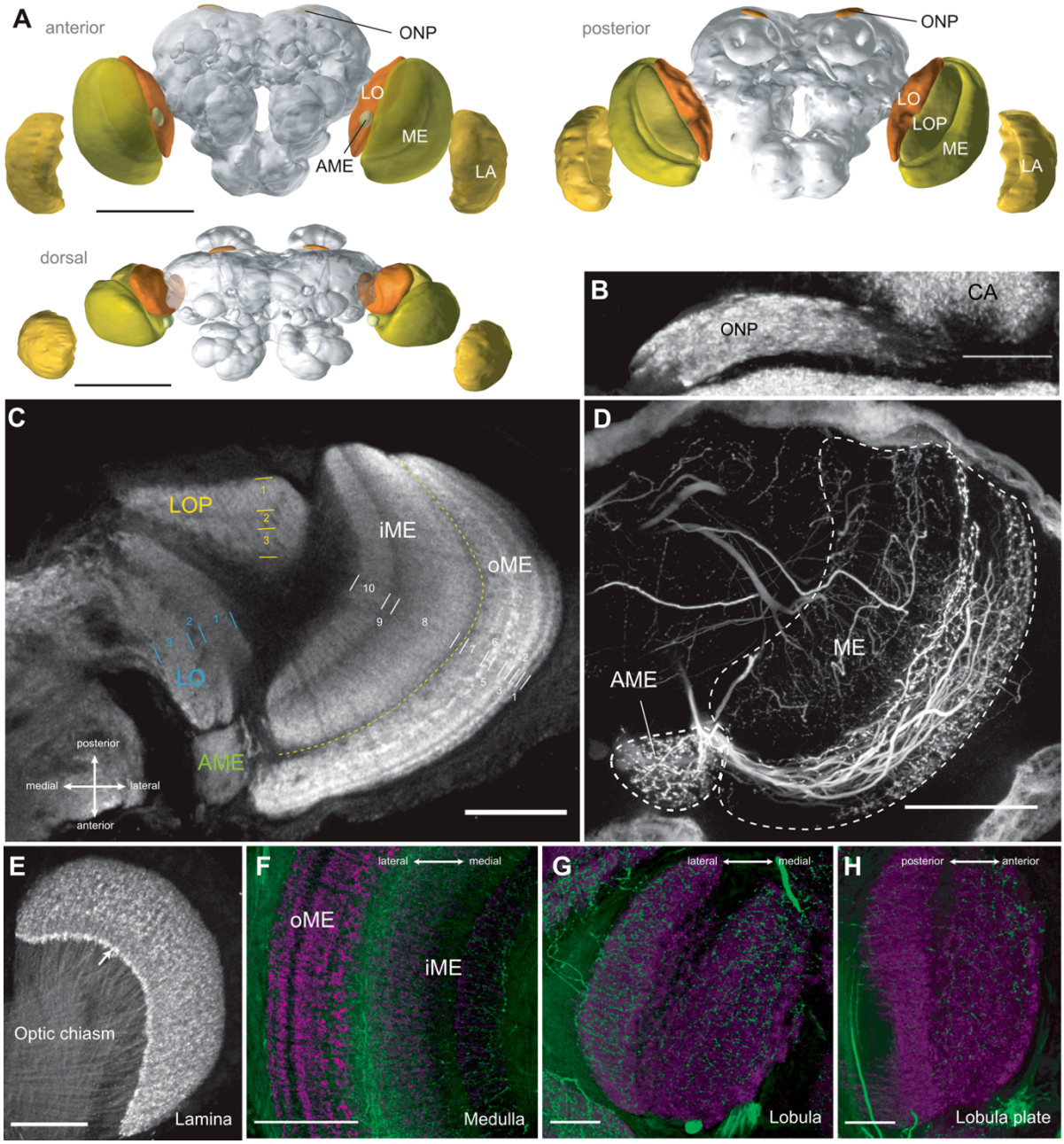

FIGURE 3 (p. 11) Primary visual neuropils. (A) Anterior, posterior and dorsal views of a 3D reconstruction showing the optic lobes including lamina (LA), medulla (ME), accessory medulla (AME), lobula (LO), lobula plate (LOP) and ocellar neuropils (ONP). (B) Left ocellar neuropil (ONP) stained against synapsin. These small neuropils are located near the dorsal surface of the Bogong moth brain and receive direct input from the ocelli via the ocellar nerve (not shown). (C) Horizontal section of the optic lobe, stained against synapsin. The 10 layers of the medulla (labelled white) are shown: the first seven layers comprise the outer medulla (oME) while layers eight to ten form the inner medulla (iME). iME and oME are separated by the serpentine layer. The lobula (LO; blue) and lobula plate (LOP; yellow) each show three distinct layers. The accessory medulla (AME; green) is located at the anterior end of the medulla. (D) Neurobiotin injection into the optic stalk shows a small subset of neurons that branch within the accessory medulla, while most other neurons branch in the medulla. (E) anti-synapsin staining of the lamina (LA), which clearly shows the inner, synapsin-rich layer. Neurons from the lamina connect to the medulla and cross over in a clearly visible optic chiasm. (F-H) Distribution of serotonergic fibres (stained with anti-5HT, green) within the medulla (E), lobula (F) and lobula plate (G). Neuropils are labelled with anti-synapsin (magenta). The serpentine layer (C) separates the inner and outer medulla, and most 5HT-positive neurons invade the medulla in this layer. Scale bar (A) 500 μm, (B, F-H) 50 μm, (C-D, E) 100 μm.

small, accessory medulla is found at the anterior margin of the lobula.

The most distal neuropil is the lamina (Figure 3A, E). It consists of two distinct layers, a thick outer layer and a thin inner layer. The latter is characterised by intense synapsin immunoreactivity. This neuropil ishe first processing stage of visual input and is connected to the second processing stage, the medulla, via the outer optic chiasm (Figure 3E). The medulla is the largest neuropil in the optic lobe and can be subdivided into an outer and inner medulla. Anti-synapsin and anti-5HT labelling demonstrates an intricate layering of both compartments. Overall, ten medulla layers can be distinguished in this way, of which seven are located in the outer medulla and three are in the inner medulla (Figure 3C). The serpentine layer separates the outer and inner medulla and provides an entry point for tangential fibres innervating both parts. This layer also exhibits the most intense 5HT labelling within the medulla, which otherwise is mostly present in the inner medulla, with only very sparse 5HT immunoreactive terminals present across the outer medulla. Separated by the inner optic chiasm, the lobula lies medially of the medulla and consists of three layers (Figure 3G). Unlike in hawkmoths, there is no pronounced separation into an outer and inner lobula (el Jundi, Huetteroth, Kurylas, & Schachtner, 2009). In line with this observation, 5HT labelling is evenly distributed across the entire neuropil. The lobula is associated with the lobula plate, which is wedged between the lobula and medulla on the posterior side of the optic lobe (Figure 3A, H). Both neuropils combined form the lobula complex, the final processing stage of visual information from the compound eyes in the optic lobe. Like the lobula, the lobula plate possesses three layers, of which the posterior-most layer shows no 5HT immunoreactivity. Finally, the small accessory medulla is located near the medial rim of the medulla, directly adjacent to the anterior margin of the lobula (Figure 3A, C, D). This neuropil has no obvious internal structure and is approximately spherical in shape. Due to numerous protrusions towards the dorsal and ventral sides it has a rather irregular appearance.

Anterior optic tubercles

The target of most optic lobe projection neurons in insects are the optic glomeruli spread throughout the ventrolateral

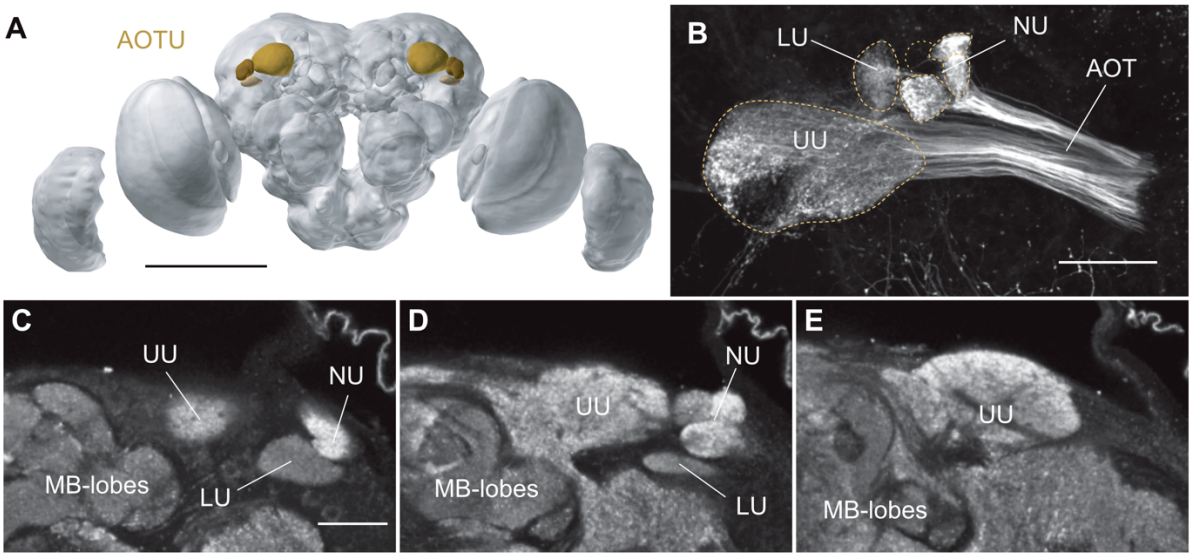

FIGURE 4 The anterior optic tubercle. (A) 3D reconstruction of the anterior optic tubercles (AOTU) in the Bogong moth brain. (B) Neurobiotin tracer injection into the optic lobe labels the upper unit (UU), lower unit (LU) and three subunits of the nodular unit (NU) of the AOTU. One subunit of the nodular unit is missing. AOT = anterior optic tract. (C-E) Optical horizontal sections through the AOTU show the upper unit, the full extent of the lower unit, and all four subunits of the nodular unit. Scale bar: (A) 500 μm, (B, C) 50 μm.

protocerebrum (Ito et al. 2014). The most prominent of these glomeruli is a well-defined region near the anterior surface of the brain. This region is called the anterior optic tubercle (AOTU, Figure 4) and represents the first processing stage of visual information reaching the central brain from the optic lobes via the anterior optic tract. In the Bogong moth, the overall layout of this neuropil was presented in de Vries et al. (2017), a study that described the neuropils underlying compass navigation in two related species of noctuid moths. Consistent with this study, we found that the AOTU is located directly underneath the anterior surface of the Bogong moth brain, dorsally of the antennal lobes and laterally of the mushroom body lobes. It consists of three subunits: the upper unit, the lower unit and the nodular unit (Figure 4B-E). The nodular unit and the lower unit together form the lower unit complex. Whereas the lower unit had a homogeneous appearance in synapsin labelling, the nodular unit was further subdivided into four compartments. The AOTUs are connected to the optic lobes via the anterior optic tract (Figure 4B). Dye injections into the optic lobe revealed that subsets of the four nodular-unit compartments are innervated by distinct optic-lobe projections. Similarly, the large upper unit receives projections that are not all homogeneously spread across the entire region, but innervate distinct ventral and dorsal aspects of this neuropil.

Antennal lobes

The antennal lobes (AL, Figure 5) receive direct input from the antennae and are the primary processing stages for olfactory information. They are situated at the anterior margin of the central brain and are subdivided into individual processing units known as olfactory glomeruli. The glomeruli occupy the periphery of the AL and surround a central neuropil region that mostly contains fibres without anti-synapsin labelling. Each glomerulus is also characterised by a centre-surround structure, highlighted by 5HT

labelling that is restricted to the core of each glomerulus (data not shown). The periphery of the glomeruli shows bright anti-synapsin labelling. In total, the Bogong moth AL contains 72-75 glomeruli (six ALs from four moths). Near the anterior side of the AL, glomeruli are of regular, round appearance, whereas they become more irregular in shape in posterior regions of the AL, in particular towards the medial edge (Figure 5B). A group of well-defined, large glomeruli near the dorsal posterior side of the AL stood out as a distinct cluster.

The ALs are the only neuropils of the Bogong moth brain that show an obvious sexual dimorphism. Three large male-specific glomeruli form the macroglomerular complex (MGC) near the entry point of the antennal nerve (Figure 5B, E). In females, the glomeruli in the same region are much smaller and cannot be distinguished from the ordinary non-MGC glomeruli. All well-defined, non MGC glomeruli could be individually matched between male and female preparations (n = 2 each). However, we found one glomerulus in females that had no identifiable counterpart in males and thus appears to be female-specific (Figure 5B). Whether this glomerulus is indeed female specific, or whether this region of the AL shows inter-individual variability with respect to glomeruli numbers remains to be shown.

Mushroom bodies

Olfactory information leaves the AL via one of several tracts that transmit information to higher brain centres. The most prominent of these second-order olfactory regions is the mushroom body, a paired set of brain regions, comprised of the calyx, the pedunculus, and a complex system of lobes. Whereas the calyx is located at the posterior brain border, the lobes occupy the anterior part of the central brain, just dorsally of the ALs (Figure 6A). The pedunculus forms the connection between both parts along the antero-posterior

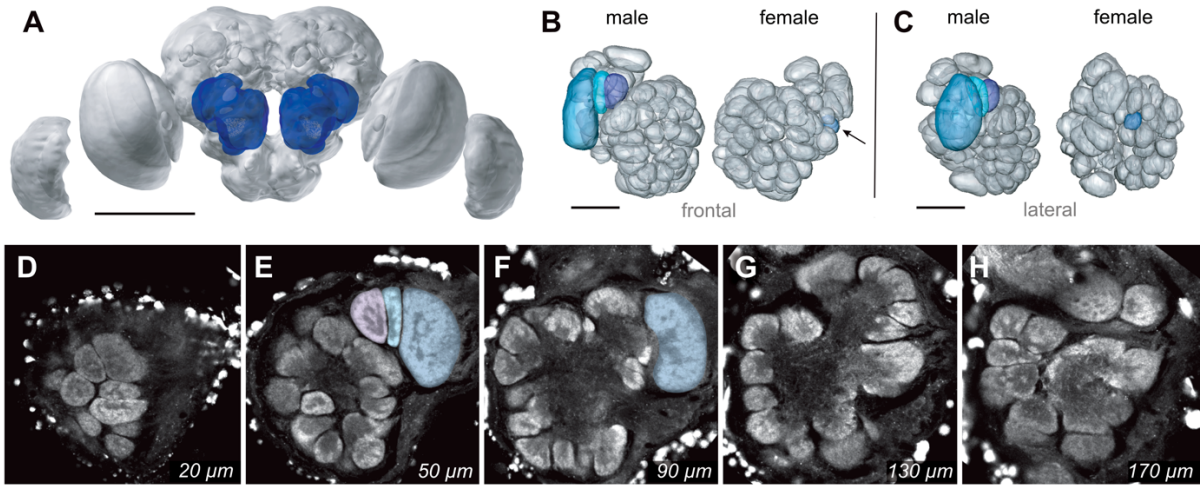

FIGURE 5 The antennal lobe. (A) 3D reconstruction of the Bogong moth brain with the antennal lobes (ALs) highlighted in blue. Scale bar = 500 μm. (B) Detailed 3D reconstruction of a male and female AL. Out of a total of 72 glomeruli in the male AL, three glomeruli were identified as macroglomeruli (highlighted in blue, turquoise and purple). Female ALs have 73 glomeruli, including one that appears to be female-specific (highlighted in blue, arrow). (C) In both males and females, anterior glomeruli appear more regularly shaped than posterior glomeruli, which are also larger. Scale bar = 100 μm. (D-H) Optical sections progressing from anterior to posterior through an anti-synapsin labelled male antennal lobe. The macroglomerular complex (MGC, glomeruli 66, 67 and 68) extends approximately from a depth of 25 μm to 120 μm, with 0 μm marking the top of the AL. The antennal nerve enters the AL at the cumulus of the MGC (glomerulus 67).

brain axis, comprising dense bundles of axons that span the entire central brain. Input from the AL reaches the mushroom body in its posterior-most compartment, the calyx. One calyx is located on each side of the brain and each consists of an outer and an inner calyx, that is, two ring-like neuropils that are fused in the centre, close to the origin of the pedunculus. Two holes are visible in the centre of both rings in anti-synapsin labelled brains and are formed by bundles of primary neurites of Kenyon cells, the principal intrinsic neurons of the mushroom body (Sjöholm, Sinakevitch, Ignell, Strausfeld, & Hansson, 2005).

The calyces are characterized by small, globular synaptic domains that are evident from anti-synapsin labelling (Figure 6G). These microglomeruli are the terminal synapses of input neurons to the calyx. Dye-injections into the AL revealed that they belong predominantly to olfactory projection neurons (Figure 6I). However, dye injections into the optic stalk demonstrated that a small set of projections originates not in the AL but in the optic lobe. Surrounding the two central holes in each hemi-calyx, these projections form a distinct inner ring that is nested within a larger outer ring, giving rise to an overall structure that consists of two sets of concentric neuropil rings in each calyx (Figure 6H). Tightly associated with the calyx is the accessory calyx, which also receives visual projections (Figure 6K, L). The accessory calyx is evident as a ventral protrusion from the calyx-proper, directly adjacent to the pedunculus. The borders of this region are not sharply defined and the neuropil is fused posteriorly with the calyx and anteriorly with the protocerebral mass that surrounds the pedunculus on its ventral side.

The pedunculus contains the axons of the Kenyon cells and links the input region of the mushroom body (calyx) to its principal output regions, the lobes. In the Bogong moth two primary lobe systems can be distinguished with synapsin labelling: the vertical and the medial lobes, each of which can be separated into two parallel sub-lobes. These two systems originate from the anterior end of the pedunculus and stretch medially towards the midline (medial lobe) and dorsally towards the dorsal brain border (vertical lobe; Figure 6C). The medial lobe contains the beta lobe and medial gamma lobe, while the vertical lobe contains the alpha lobe and the vertical gamma lobe (Figure 6D-E). Towards their distal ends, the beta lobe as well as the alpha lobe further separate into two parallel neuropil streams, likely corresponding to the alpha and alpha-prime, and the beta and beta-prime compartments known from other species (e.g. Sjöholm et al., 2005). Both lobe systems have a complex, convoluted structure towards the anterior brain surface, where the two arms of the gamma lobes meet and wrap around the roots of the beta and alpha lobes. In particular the ventro-lateral regions of the medial lobe have numerous protrusions and sub-lobes and it is not always obvious where the exact border between the alpha lobe and the overlaying gamma lobe is. Near the point where the vertical and medial lobes have their common root, we found another small neuropil that could not be assigned to one of the two lobes. This spherical region was called the spur and might indeed correspond to the spur region in *Drosophila* (Ito et al. 2014; Figure 6M, N).

Finally, as other lepidopteran insects, the Bogong moth also has a secondary lobe system with a separate connection to the calyx, the Y-tract (Figure 6F). This tract originates in dorsal regions of the calyx and

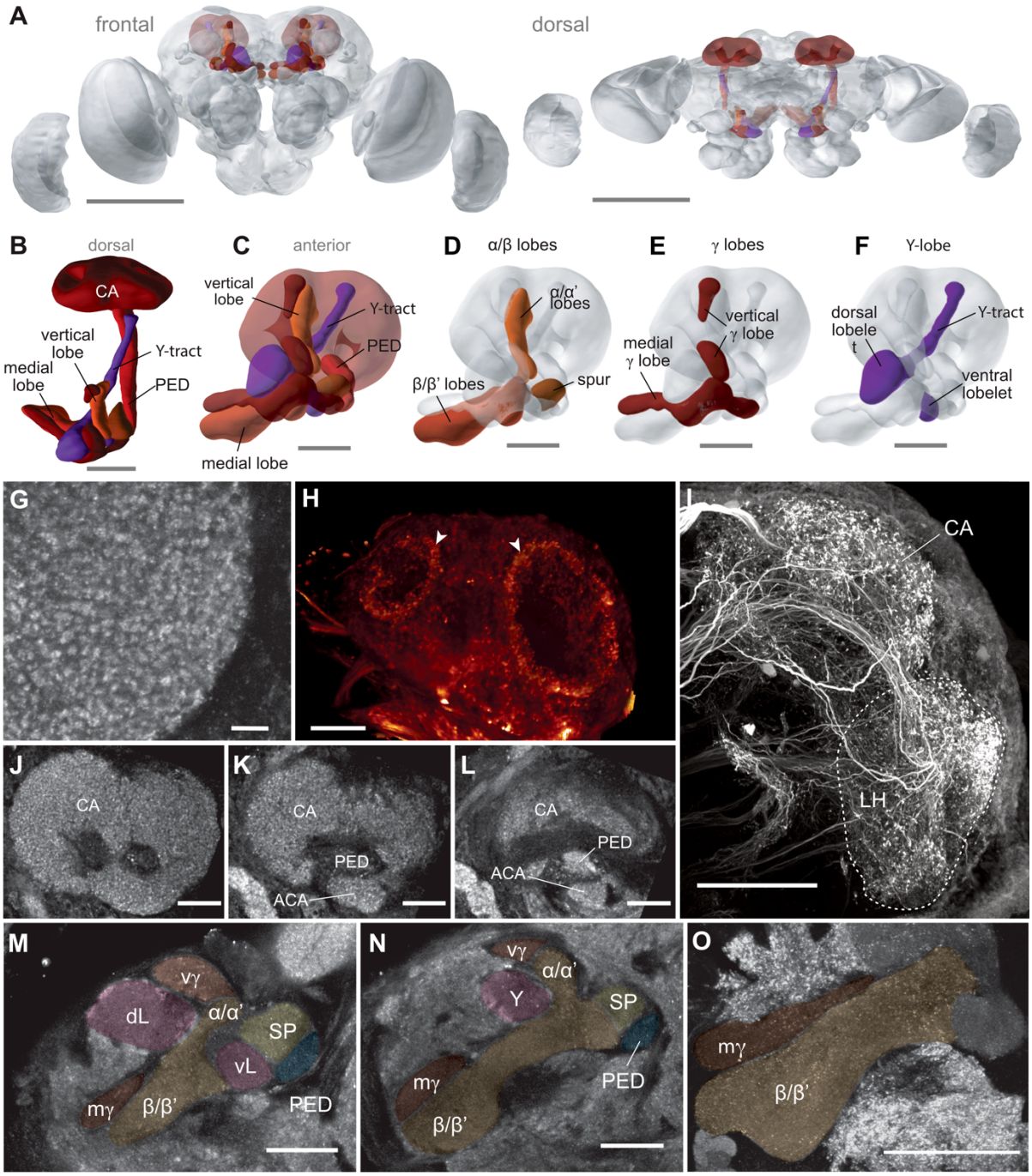

FIGURE 6 The anatomy of the mushroom body. (A) 3D reconstruction of the mushroom bodies (MBs) within the brain, frontal and dorsal view. The MBs span from the frontally-located lobes to the dorsal calyces. (B) Lateral view of the MB. (C) Frontal view of the MB. (D-F) Frontal view of the MB, with the three lobe systems highlighted. Scale bar = 100 μm. (G) The calyx is composed of clearly visible micro-glomeruli. Scale bar = 10 μm. (H) Injection of Neurobiotin into the optic stalk highlights neurons with output in the inner ring of the calyx (volume rendering of confocal image stack). (I) Neurobiotin injection into the antennal lobe labels projection neurons to the calyx of the MB and the lateral horn (LH). (J-L) Frontal optical sections (10 μm steps) through the calyx reveal the peduncle and accessory calyx. (M) Frontal section through the MB lobe systems at a depth of 90 μm. my = medial gamma lobe, ß/ß' = medial beta lobes, vy = vertical gamma lobe, dL = dorsal lobelet of the y-lobe, vL = ventral lobelet of the y-lobe, Sp = spur, Ped = peduncle. (N) Frontal section through the MB lobe systems at a depth of 130 μm. a/a' = medial alpha lobes. (O) Frontal optical section through the medial beta/beta' lobe and medial gamma lobe (maximum intensity projection over 10 steps, step size = 1 μm). Scale bars in A = 500 μm, B-F, G, M = 100 μm, H-L, O-P = 50 μm.

runs parallel to the pedunculus towards the anterior side of the brain. It turns medially just posteriorly of the vertical lobe and supplies two lobelets that intermingle with the main lobe systems (Figure 6M, N). The ventral lobelet of the Y-lobe is comparably small and sharply defined. It protrudes through the beta lobe towards the ventral margin of the lobe system, where it borders the AL and the lateral accessory lobes (LAL). The dorsal lobelet is much bigger and fills large portions of the space stretching in between the vertical and medial lobes, expanding all the way to the anterior brain surface. This lobelet corresponds to the largest of three ellipsoid mushroom body lobe protrusions that are visible as landmarks on the brain surface. The remaining two are formed by the vertical and medial gamma lobes.

The second major target region for olfactory projections from the AL is the lateral horn (Figure 6I). The neurons terminating in the lateral horn either originate in the medial antennal lobe tract and reach the lateral horn after providing input to the calyx, or they target this region directly via the lateral and mediolateral antennal lobe tracts (Ian, Berg, Lillevoll, & Berg, 2016). The lateral horn neuropil is located in the lateral-most part of the central brain and is medially completely fused with the surrounding protocerebral regions (inferior, superior and ventrolateral protocerebrum). Dye injections into the AL revealed the location and approximate size of this area (Figure 6I), but further analysis will be required to delineate the exact borders of the lateral horn.

Central complex

Together with the AOTU and the lateral complex, the central complex (CX) of the Bogong moth brain was examined in a previous study (de Vries et al., 2017) in the context of potential roles of these neuropil groups for migratory behaviour. As this study was focused on identifying volumetric correlates of migratory lifestyle, it did not describe the detailed neuroanatomical features of the Bogong moth CX, which was therefore the aim of the current study.

The CX is a midline-spanning group of neuropils, located dorsally of the oesophageal foramen. It consists of four compartments: the protocerebral bridge (PB), the noduli and the central body. While the central body is the only unpaired neuropil in the brain (Figure 7A, B), both the PB and the noduli occur in symmetrical pairs on either side of the midline. The central body is composed of the fan-shaped body (FB; or central body upper division, CBU) and the ellipsoid body (EB; or central body lower division, CBL). The EB is the anterior-most CX compartment and has a bar-like shape, with its ends bent slightly anteriorly. It spans the width of the central body from right to left and has clearly defined borders on all sides. The FB is directly adjacent to the EB on its posterior side and partially encompasses the EB from behind. It is approximately three times as large as the EB and has a pronounced stratified appearance (Figure 7D-G). Posterior to the FB, at the posterior border of the brain, lies the PB. The FB and the PB are separated by a stretch of neuropil belonging to the inferior protocerebrum that possesses two large openings on either side of the midline, allowing the passage of neurites between the two CX compartments. Each PB-hemisphere is visible as a brightly synapsin-labelled, hook-like structure (Figure 7K). It emerges near the midline, bends dorsally, and then continues ventro-laterally in a straight line, approximately to the level of the mushroom body pedunculus. The medial parts of the PB have a larger diameter, which continually

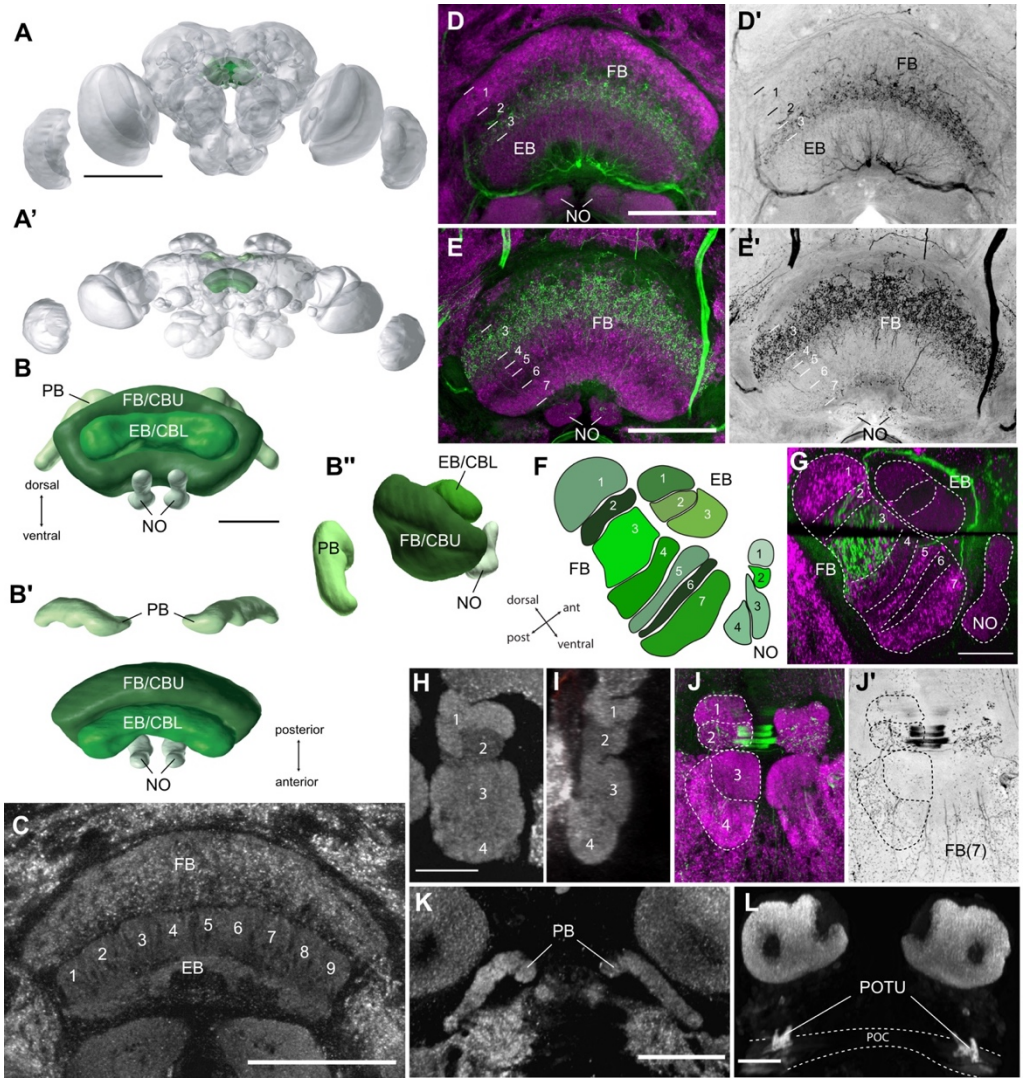

FIGURE 7 The morphology of the central complex. (A) Frontal view of a 3D reconstruction of the Bogong moth brain, with the central complex (CX) highlighted in green. Scale bar = 500 μm. (A') Dorsal view of the same reconstruction. (B-B'') 3D reconstruction of the CX, frontal view (B), dorsal view (B'), and lateral view (B''). Scale bar = 100 μm. (C) Frontal confocal section of the CX, highlighting the ellipsoid body (EB and its clearly visible lateral slices. Scale = 100 μm. (D) Anti-synapsin (magenta) and anti-5HT (green) staining highlight the layers of the fanshaped body (FB). Shown is a maximal intensity projection (depth 5 μm) at the level of the EB and layer 1-3 of the FB. Scale = 100 μm. (D') 5HT labelling from D, isolated and shown with inverted colormap. (E,E') As D and D', but for a cross-section at a more posterior level, showing layers 3-7 of the FB as well as 5HT labing in the noduli (NO). (F) Schematic cross-section of the central body and noduli. The FB has seven layers defined via anti-synapsin and anti 5HT labelling. The three layers of the EB are visible as well as all four subunits of the noduli. (G) Sagittal cross-section of FB showing the 7 individual layers (maximal intensity projection, 12 images, step size = 0.4 μm); compound image from two physical thick-sections. The black gap across the FB is the border of the two slices. Scale = 100 μm. (H) The paired noduli have four subunits each, visible in this horizontal confocal section. Scale bar = 50 μm. (I) Sagittal view of the same preparation as in (H). (J) Maximal intensity projection of a preparation labelled against synapsin and 5HT, revealing the 5HT labelling in layer 2 of each nodulus. (J') Isolated 5HT labelling from (J), highlighting the serotonergic innervation of layer 2, as well as the small, beaded terminals of FB layer 7 (partly superimposing the ventral layers of the noduli). (K) Frontal view of the protocerebral bridge (PB; maximal intensity projection, 10 images, step size = 1 μm). Scale = 100 μm. (L) Frontal view of the posterior optic tubercle (POTU). Maximal intensity projection (16 images, step size = 2 μm) showing the POTU located posterior to the posterior optic commissure (POC). Scale = 50 μm.

decreases towards the lateral ends. The final lateral segment of the PB often stands out as a distinct, globular domain. A thick fibre bundle interconnects the right and left PB across the midline. The final CX neuropils, the noduli (NO), are located ventrally of the FB and the EB. These neuropils are the smallest part of the CX and consist of a large and a small compartment, both of which are separable into two layers (Figure 7H-J).

Given the complexity of the neuroarchitecture of the CX, the tight structure-function relations in this region across insects, and its likely role as an internal compass also in the Bogong moth, we will highlight the distinguishing features of each of the CX compartments. Most prominently, the FB exhibits a pronounced stratification that was revealed via a combination of synapsin labelling and anti 5HT labelling. Using these techniques as defining markers, this neuropil is subdivided into seven layers (Figure 7D-G). These layers are linearly stacked on top of each other from dorsal to ventral. Layer 1 is easily distinguished by its arch like morphology and the brightest synapsin labelling within the FB. Adjacent ventrally is layer 2 and 3, showing weaker synapsin labelling. Layer 3 is a thick, strongly serotonergic stratum, characterized by large, beaded 5HT positive terminals (Figure 7E). The overlaying thin layer 2 shows only weak 5HT labelling, which originates from 5HT-labelled fibres that pass through this layer. The ventral half of the FB contains weaker 5HT labelling visible in two out of the four remaining layers. We distinguished four layers (4, 5, 6 and 7) according to differences in the visual appearance of synapsin labelling and the presence of 5HT labelling (Figure 7E', F). Unlike the FB, the second part of the central body, the EB, has a less pronounced stratification (Figure 7C,D). 5HT labelling was found evenly distributed in the EB but was less distinct than in the FB. Based on synapsin labelling, three layers were identified. The dorsal-most layer was distinguished from the remaining EB due to the presence of nine clearly delineated lateral divisions, i.e. slices (Figure 7C). A columnar structure was partially visible in the PB as well, but was more obvious in lateral parts of the neuropil. Towards the midline, columns fuse into a homogeneous neuropil without any internal features. Finally, the noduli consist of four layers each, two in the small dorsal compartment and two in the larger ventral compartment. The first layer forms a cap-like region of bright synapsin labelling, while the remaining three layers are less clearly delineated (Figure 7H-J). Layer 2 of the noduli shows sparse innervation by serotonin-immunoreactive beaded fibres (Figure 7J), which were labelled in varying intensity between individual preparations.

A region closely associated with the PB is the posterior optic tubercle (POTU; Figure 7L). While not strictly part of the CX, this irregularly shaped neuropil is located at the posterior surface of the brain on either side of the midline. It is connected to the PB via two thin fibre bundles, which extend beyond the length of the PB towards ventrolateral directions. The POTU is located at the intersection of this bundle and the horizontally running posterior optic commissure (POC, Figure 7L), a major commissure interconnecting the optic lobes on either side of the brain.

Lateral complex

The final set of well-defined neuropils in the Bogong moth brain is the lateral complex. This brain area consists of three distinct compartments and is located immediately adjacent to the CX, flanking it laterally and

ventrally on both sides. It stretches from the level of the central body towards the anterior brain surface and borders anteriorly with the AL and the mushroom body lobes. Each lateral complex consists of the large lateral accessory lobe (LAL), complemented by the smaller bulb and the gall, which are situated on the anterio-dorsal surface of the LAL (Figure 8A, B).

The borders of the LAL are well defined along its anterior and medial margins. In those regions it is bordered by the AL (anteriorly) and the medial antennal lobe tract (medially). The lateral boundary is evident with the help of anti-5HT labelling, which highlights a pronounced difference in staining pattern and intensity between the bordering ventrolateral protocerebrum and the lateral portions of the LAL (Figure 8C, D). Dorsally, the bulb, the isthmus tracts and the mushroom body lobes create natural boundaries in most regions, which can be generalized into a dorsal cut-off plane for more ambiguous areas near the anterior brain surface and the posterior extremes of the LAL. The posterior boundary is defined by the horizontal crossing of the lateral antennal lobe tract behind the LAL, which defines the plane that separates the LAL from the more posterior regions of the ventromedial protocerebrum. While this border is somewhat arbitrary, it is consistent with the LAL definitions in other species (Heinze & Reppert, 2012; Immonen et al., 2017; Ito et al., 2014). More clearly defined than the LAL, the bulb is wedged between the dorsal LAL margin and the posterio-medial surface of the mushroom body lobes (Figure 8I-K). It provides a cap-like endpoint to the isthmus tracts, which are fibre bundles that emerge from the lateral edges of the EB. As in other insects, the bulbs are thus tightly linked to the EB. Just antero-ventrally of the bulb is the gall, which is served by a subset of isthmus tract fibres that continues beyond the bulbs.

The largest compartment of the lateral complex, the LAL is further subdivided into the upper LAL and lower LAL by the inter-LAL tract (Figure 8F), which connects the two lateral complexes. The two compartments differ in their internal structure, innervation patterns of serotonergic fibres, and extent of fusion with neighbouring regions (Figure 8C, D). While the upper LAL contains numerous, irregularly shaped glomerular domains that light up brightly with anti-synapsin labelling (Figure 8G), no such internal structure was observed in the lower LAL. The borders of the upper LAL are more distinct than those of the lower LAL, which merges with the surrounding ventrolateral neuropils. Future functional data will thus have to show whether the borders of the lower LAL, although consistent with other insects, indeed represent a functional unit.

While the bulb has no easily discernible subunits, the gall contains two equally sized compartments (Figure 8I-L), each of which is targeted by a set of columnar neurons from the EB (CL1 or E-PG neurons; Figure 8L). These gall compartments have an appearance not unlike AL glomeruli, with a dark, synapsin-deficient core and a synapsin-rich rind. No finer scale structure is visible within these regions. This is in stark contrast to the bulbs, which exclusively consist of sharply defined, ball-like synaptic domains. These microglomeruli are highly visible in Azur II–Methylene Blue staining (Figure 8H), but are also apparent with synapsin immunolabeling, which is concentrated in ring-like domains surrounding the periphery of each microglomerulus (Figure 8I-K).

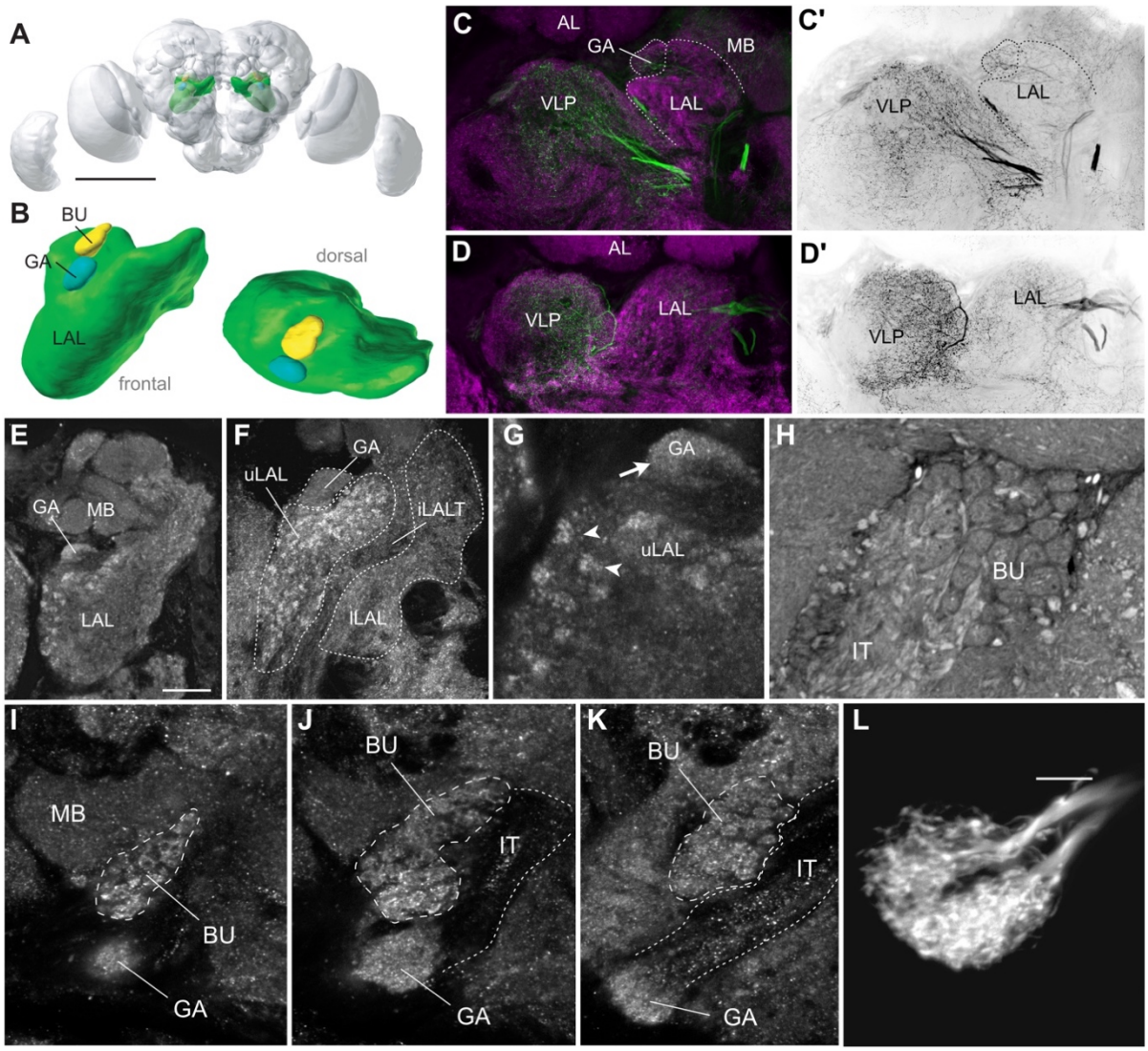

FIGURE 8 The morphology of the lateral complex. (A) 3D reconstruction of the lateral complex in the Bogong moth brain. Scale bar = 500 μm. (B) Frontal and dorsal view of the lateral complex, with the lateral accessory lobes (LALs) in green, the bulb (BU) in yellow and the gall (GA) in turquoise. (C, C', D, D') Horizontal section of the LAL showing a clear boundary to the heavily serotonin-labelled ventrolateral protocerebrum (VLP). The two sections are 120 μm apart. Anti-synapsin labelling is shown in magenta, anti-5HT staining in green. (E) The LAL lies immediately adjacent to the mushroom body lobes, with the gall nestled between the two neuropils. Scale = 50 μm. (F) The inter-LAL tract (iLALT) subdivides the LAL into the upper LAL (uLAL) and the lower LAL (lLAL). Scale bar = 50 μm. (G) Anti-synapsin stained microglomeruli in the dorsal shell of the LAL. Scale = 50 μm. (H) Light microscope image of the bulb stained with Azur II-Blue, with individual microglomeruli visible. (I-K) Horizontal optical sections showing the bulb and gall lying on top of the dorsal shell of the LAL, sections progress from dorsal to ventral. Both neuropils are served by fibres in the isthmus tract (IT). Scale bar = 20 μm. (L) Neurobiotin-labelled CL1 cell branching in the gall. The two subdivisions of the gall are clearly visible. Scale bar = 10 μm.

Discussion

Bogong moths are remarkable long-distance navigators. Yet, all navigational decisions across many hundreds of kilometres are initiated by a comparably simple brain. Understanding the neural circuitry of this brain will provide a unique window into the

neural basis of long-distance migration carried out during the night. With the current study, we have provided a morphological framework for future functional work that aims at understanding the neural basis of migration and navigation in the Bogong moth. This framework will be an essential resource for mapping projection patterns of neurons, allowing us to extrapolate fundamental properties of neural networks. It will also allow for more specific targeting of brain regions using electrophysiological or imaging techniques, and provide an important ground truth for gene expression studies.

In general, the Bogong moth brain is similar in its overall organisation to the brains of other lepidopteran insects, such as the Monarch butterfly *Danaus plexippus* (Heinze & Reppert, 2012), *Heliothis virescens* (Kvello, Løfaldli, Rybak, Menzel, & Mustaparta, 2009), *Manduca sexta* (el Jundi et al., 2009), or the hummingbird hawkmoth *Macroglossum stellatarum* (Stöckl et al. 2016). Given the spectacular migratory lifestyle of the Bogong moth, it is noteworthy that there is no single gross morphological feature of the brain that stands out as unique or different compared to related species. In contrast, it shares not only all major features of the overall insect brain ground pattern, it also exhibits all distinguishing characteristics of other lepidopteran brains. These include a suboesophageal ganglion that is fused with the brain, well-developed optic lobes, large antennal lobes, a complex organization of the mushroom body with a multi-layered double calyx and an intricately organized lobe system. One feature of the mushroom body in particular appears to be a defining characteristic of moths and butterflies, namely the presence of the Y-tract with its associated lobelets (Heinze and Reppert 2012; Sjöholm et al. 2005; Montgomery et al. 2016; Homberg et al. 1988). A second unusual feature of lepidopteran brains is that the PB of the CX is split across the midline, in contrast to other insects, in which this neuropil forms a continuous, midline-spanning structure (Heinze and Reppert 2012; Stöckl et al. 2016; el Jundi et al. 2009).

With 25 separately segmented neuropils, our average atlas of the Bogong moth brain is the most detailed reconstruction of a moth brain to date (el Jundi et al. 2009; Kvello et al. 2009; Stöckl et al. 2016). It was carried out in exactly the same way as the reconstruction of the Monarch butterfly brain (Heinze & Reppert, 2012), thus offering the basis for detailed comparisons between a day-active migratory butterfly and a night-active migratory moth.

Primary sensory brain areas

Two sensory modalities have been shown to play a role in choosing a bearing during the long range flights of both the Bogong moth and the Monarch butterfly: visual cues and geomagnetic cues (Dreyer et al. 2018; Guerra et al. 2014). Additionally, olfactory information has been proposed to be the decisive factor during the last segment of the migration, i.e. when locating the overwintering grounds or the aestivating caves (Warrant et al. 2016; Mouritsen et al. 2013). Although the sensors of magnetic field cues are unknown in any species, the antennae have been implicated in magnetosensation in the Monarch butterfly (Guerra et al. 2014), while a vision based mechanism to detect magnetic field properties remains a main hypothesis across many animal species (Ritz et al. 2000; Schulten et al. 1978), including in the Bogong moth. In any case, the processing of visual information, geomagnetic information, and olfactory cues would all involve either the antennal lobes or the

primary visual brain centres, most prominently the optic lobes. This provided our main motivation to compare these regions between the Bogong moth and the Monarch butterfly, with the aim of identifying potential specializations related to migratory behaviour.

In the Bogong moth antennal lobes we found a pronounced sexual dimorphism, highly reminiscent of other moths, but unlike the Monarch butterfly, in which both sexes showed an identical AL layout (Heinze & Reppert, 2012). In other moths, including the closely related *Agrotis segetum* and *A. ipsilon*, the male-specific part of the AL (the MGC) has been shown to process female pheromones (Hansson et al. 1994; Jarriault et al. 2010; Berg et al. 2002). Although the pheromone of the Bogong moth has yet to be identified, it is likely that pheromone-based communication exists in the Bogong moth and that the male specific MGC serves the same function as in the other species. In the context of migration, Bogong moths might pinpoint their aestivation caves based on odour cues that were left by previous generations of moths, such as excrement on the cave walls, and moth debris on the cave floor (Warrant et al. 2016; Dreyer et al., in preparation). As both male and female moths are faced with this identical challenge, the MGC, as well as any female specific glomeruli, are not expected to play a role in this guidance behaviour. Interestingly, several large glomeruli stand out near the dorso-posterior side of the AL in both sexes, similar to a group of posterior dorsal glomeruli in the Monarch butterfly (Heinze & Reppert, 2012). This group of glomeruli likely corresponds to the PD cluster described in *Bombyx mori* (Kazawa et al., 2009) and might also be present in other moths (Skiri, Rø, Berg, & Mustaparta, 2005). However, these glomeruli form a more distinct, segregated cluster in both the Monarch butterfly as well as in the Bogong moth, potentially suggesting a functional specialization. This might provide a starting point for a more detailed correlative and functional analysis aimed at locating neural specialisations that could mediate the remarkable ability of migratory lepidopteran insects to identify the highly specific, yet unfamiliar target sites of their migratory journey.

The primary visual areas of the Bogong moth brain are the optic lobes and the ocellar neuropils. Morphologically, the optic lobes of the Bogong moth have a structure similar to those of the Monarch butterfly (Heinze & Reppert, 2012) and indeed most other insects (Strausfeld 2012). They possess a configuration of five neuropils that is shared across many species, consisting of the lamina, medulla, a lobula complex composed of the lobula and the lobula plate, and the accessory medulla. As expected from the nocturnal lifestyle of the Bogong moth, the total relative volume of the optic lobe is about 50% smaller than in the diurnal Monarch butterfly, consistent with data on other butterflies (Montgomery et al. 2016). Interestingly, despite the overall size difference, the internal layout of each optic lobe neuropil is remarkably conserved between the two species. Using synapsin labelling as a marker, we found the same number of layers in all neuropils and the visual appearance of neuropils was highly consistent between species (Heinze & Reppert, 2012).

The second primary visual centres in the Bogong moth brains are the ocellar neuropils. These regions process input from the ocelli, the small lens eyes located dorsolaterally on the moth's head. In arctiid and noctuid moths, the ocelli mediate diurnal activity patterns by measuring ambient light

levels (Eaton et al. 1983; Wunderer and de Kramer 1989). However, in dragonflies the ocelli play a role in flight control (Stange, 1981), and the ocelli of several nocturnal bees and wasps have the potential to detect polarised light, suggesting a possible role in navigation (Zeil et al. 2014). Whether Bogong moth ocelli have the spectral sensitivity and photoreceptor arrangement necessary to sense polarised light remains to be determined. While the Monarch butterfly also possesses very small lateral ocelli, as well as an associated neuropil near the dorsal brain surface (personal observations), no details about these structures have been described. A potential role for detecting migration-relevant cues cannot be excluded for either species, but given the small size of these eyes, visual information would likely be limited to sensing illumination levels and, potentially, spectral composition and polarisation angles of skylight cues.

An interesting alternative role for both the optic lobe and the ocellar neuropils arises from the finding that the Bogong moth is able to use the geomagnetic field as a compass cue (Dreyer et al., 2018). The location of the magnetic sense and the identity of the sensor are currently unknown, but similar to proposals in migratory birds, magnetic information might be detected via a radical-pair based mechanism mediated by a blue-light receptor molecule called cryptochrome (Schulten et al. 1978; Ritz et al. 2000). In fact, the highly regular subcellular organization of photoreceptor cells would be an ideal substrate for a hypothetical magnetoreceptor. Beyond the retina, the optic lobes would then be a convenient access point to study neural responses to changes in the magnetic field. The ocellar retina has not yet been investigated with respect to the presence of a light-activated cryptochrome, and thus remains a potentially intriguing site for physiological and immunohistochemical studies, both with respect to visually-guided navigation and as a potential substrate for a visual magnetic sense.

Overall, while all primary processing stages for visual and olfactory information are highly developed in the Bogong moth, we found no obvious specializations that would suggest a specific role during migration. Similarities and differences between the Bogong moth and the Monarch butterfly appear to be linked to the diurnal versus nocturnal lifestyle and the location of these species on the lepidopteran phylogenetic tree. While a potential role in magnetoreception for the visual neuropils is a fascinating idea, we could neither support nor dismiss this possibility based on our anatomical data.

Anterior optic tubercles

The Bogong moth AOTU receives input from the optic lobes via the anterior optic tract and constitutes the only anatomically distinct direct target region of optic lobe projection neurons. While this region is present in all insects that have been studied to date, the morphological composition of the AOTU differs between species and is less conserved compared to the optic lobes. Generally, two main subunits are present in the AOTU: a large upper unit and a smaller, more diverse lower unit complex (LUC). The LUC can consist of only one region (e.g. in locusts: (Homberg, Hofer, Pfeiffer, & Gebhardt, 2003), or consist of several components with more or less defined internal borders (in bees: Mota et al. 2011; Zeller et al. 2015; in dung beetles: Immonen et al. 2017).

Within the Lepidoptera, a large upper unit and two main LUC compartments can generally be identified (el Jundi et al., 2009; Heinze & Reppert, 2012). The latter are the

lower unit and the nodular unit. Between species there are differences in the specific composition of these subunits. While the nodular unit of the Bogong moth AOTU has four compartments, only three were found in the Monarch butterfly (Heinze & Reppert, 2012). Furthermore, the lower unit of the Monarch butterfly extends into an elongated structure called the strap, which is not present in the Bogong moth. As the AOTU of the neotropical butterfly *Godyris zavaleta* possesses an internal composition similar to that of the Monarch butterfly (Montgomery et al., 2016), the differences in LUC structure are either due to phylogenetic constraints or driven by higher visual demands in response to the butterfly's day-active lifestyle. The finding that the AOTU of the diurnal hawkmoth *Macroglossum stellatarum* was very similar to that of other moths (Stöckl et al. 2016) points to phylogeny as the most important factor determining the differences within lepidopteran insects. Detailed investigations comparing size differences in the various AOTU divisions revealed the larger size of the upper unit in day-active species as the only consistent trend that was valid across species (Stöckl et al. 2016; de Vries et al. 2017). Additionally, a smaller lower unit was found in the day-active migrant *M. stellatarum* compared to the nocturnal non-migrant *Deilephila elpenor* (Stöckl et al. 2016), while a larger nodular unit was found in the Bogong moth compared to its close relative *Agrotis segetum* (de Vries et al., 2017).

Functionally, studies in the desert locust and Monarch butterfly showed that the AOTU-LUC is an important processing stage for polarised light and sun position information (Pfeiffer et al. 2005; Pfeiffer and Homberg 2007; Heinze and Reppert 2011). For these long distance migratory insects, the angle of polarised skylight serves as a compass cue and can be used to determine the insects' heading direction. Their AOTU contains at least two parallel pathways passing through the different regions of the LUC, carrying physiologically distinct information (Heinze, 2014). In *Drosophila*, two similar parallel pathways encode different aspects of landmark information and also pass through the LUC of the AOTU (Omoto et al., 2017; Shiozaki & Kazama, 2017). In all species, these pathways share the bulbs of the lateral complex as their sole target and thus provide input to the head-direction system of the CX, suggesting that this is also the case in the Bogong moth.

Which sensory information can be used as a direction signal for a nocturnal animal like the Bogong moth? Polarised light from the sun is available until the sun is 18° below the horizon, thus until approximately one hour after sunset (Cronin et al. 2006). Aestivating Bogong moths have been observed to swarm in the hour after sunset, and they appear to depart on their migration within this time as well (Common, 1954). Thus, polarised light from the sun may be a viable directional cue during the first hour of flight. Later at night, polarised light from the moon can also be used for course control, and possibly the moon's position itself as well as the Milky Way could be integrated to inform the compass system (Warrant and Dacke 2016). Independent of which compass cues are used for migration in the Bogong moth, all are likely relayed via the LUC of the AOTU, as this is the only currently known pathway providing allothetic sensory input to the head direction system of the CX. Given the importance of the task, the moths can be expected to use every cue that is available to them to choose a stable flight direction, from landmarks and visual compass cues to

magnetic field information. Being a likely processing station for these cues, the AOTU is a primary target for physiological studies of the sensory basis for migratory behaviour in the Bogong moth.

Central and lateral complex

The CX is the brain region most heavily involved in spatial orientation and navigation, and it is therefore likely crucial during the Bogong moth's migration (de Vries et al., 2017). It is anatomically conserved throughout the insects, likely because of its fundamental function in spatial orientation. As in all insects, the Bogong moth CX consists of the fan-shaped body (FB, or CBU), the ellipsoid body (EB, or CBL), the protocerebral bridge (PB) and the noduli (NO). The EB is visibly divided into 9 lateral columns, identically to the locust (Williams, 1975) and the dung beetle (el Jundi, Baird, Byrne, & Dacke, 2019). In the butterfly, locust, fruit fly and beetle, this columnar structure has been shown to result from a highly conserved underlying neural organisation (el Jundi et al., 2019; Heinze, Florman, Asokaraj, el Jundi, & Reppert, 2013; Heinze & Homberg, 2008; Wolff, Iyer, & Rubin, 2015). These columnar neurons form the basis of a neural circuit that uses both external and internal sensory cues to encode heading direction (Green et al., 2017; Turner-Evans et al., 2017). In two other long-distance migrating insects, the Monarch butterfly or the desert locust, this circuit uses the Sun's position and the skylight polarization pattern as the key cues to encode heading in a global reference frame (Heinze and Reppert 2011; Homberg 2015). In flies and cockroaches, local landmarks have been shown to be used to compute heading (Seelig & Jayaraman, 2013; Varga & Ritzmann, 2016). Importantly, in both species the head direction system also operates in darkness, using internal information like the angular velocity of the fly's movement to compute a heading estimate (Turner-Evans et al., 2017). The high degree of functional and anatomical conservation of this circuit across a wide range of insects suggests that the corresponding cells in the Bogong moth CX also encode heading in this species. Whereas the close resemblance of the CX layout between the Bogong moth and the Monarch butterfly likely reflects functional correspondence, we can neither infer which cues are used to encode heading nor whether a heading signal is tethered to a global or a local reference frame. However, our detailed description of the CX neuropils, combined with the available behavioural data, provides a solid starting point to functionally explore the heading direction system used to guide the nocturnal migrations of the Bogong moths.

Beyond knowing the heading, the moths also have to know their target direction during the migratory journey. Based on a computational model that describes the CX as a neural substrate for path integration (Stone et al., 2017), it was recently suggested that this network could be modified to produce migratory behaviour (Honkanen, Adden, da Silva Freitas, & Heinze, 2019). The proposed model contains a set of memory neurons whose combined activity encodes the home vector in a path-integrating insect, generating an activity peak that signals the current nest direction and which is used by a steering cell population to keep the insect on track. While this activity peak dynamically changes with the ever-changing home vector, a migratory heading needs to be fixed and genetically encoded. In migratory insects like the Bogong moth, this could in theory be accomplished by fixing the synaptic weights of the neurons corresponding to the memory cells, so that

their population generates a constant output signal causing the animal to steer into the migratory heading whenever it is moving (Honkanen et al., 2019). Although experimentally challenging, the predicted activity patterns as well as the potential synaptic weight distributions are testable, and the detailed descriptions of the brain regions involved that we have provided in our current study lay the groundwork for these studies.

Finally, the CX gives direct output to the lateral accessory lobes (LALs), a brain region that has been implicated in (and is ideally located for) initiating behaviours: pre-motor neurons descend from this region into the ventral nerve cord and are known to directly control steering in the silkworm moth (Namiki & Kanzaki, 2016). During migration, steering precisely towards the target is crucial, as even small mistakes may result in missing the target completely and would therefore be fatal for the moth. The Bogong moth LAL is anatomically very similar to that of the silkworm moth (Iwano et al., 2010). Furthermore, neurons that were described to play a role in phonotactic steering in crickets (Zorovic & Hedwig, 2011) closely resemble the ones involved in steering in the silkworm moth, suggesting that the circuit is indeed widely conserved. The Bogong moth LALs are therefore a likely substrate for a similar steering circuit, which can now be probed by electrophysiological recordings.

Mushroom bodies

Besides the CX, the mushroom bodies (MBs) are the second major integration centre in the insect brain. This region is tightly associated with olfactory memory (Strausfeld et al. 1998), but in many species also receives input from other modalities, such as vision (Gronenberg 2001; Lin and Strausfeld 2012; Paulk and Gronenberg 2008). In principle, the mushroom body forms a large association matrix that correlates sensory input with reward signals. During this process, synaptic weights are adjusted, so that the likelihood of rewarded sensory signals driving the output neurons of the mushroom body is increased after learning. That way, sensory information is given a valence based on previous experience (Aso et al., 2014; Menzel, 2014; Strube-Bloss, Nawrot, & Menzel, 2011). The two main parts of the mushroom body are the calyx and the lobes, with the calyx being the site of sensory input and the lobes being the site of modulatory input and the origin of output signals (Strausfeld, Sinakevitch, Brown, & Farris, 2009). Thousands of parallel Kenyon cells with input in the calyx and output in the lobes form the backbone of the mushroom body association matrix. Different sets of Kenyon cells form separate, functionally distinct lobe systems, for example the alpha/beta lobes, and the alpha'/beta' lobes. In most insects the two components of each of these systems are anatomically distinct and located in the vertical lobe (alpha/alpha') and the medial lobes (beta/beta'), giving each Kenyon cell a bifurcated appearance (Sjöholm et al., 2005; Strausfeld et al., 2009).

In the Bogong moth the mushroom bodies are very similar to those described in other lepidoptera (Strausfeld et al. 1998; Sjöholm et al. 2005; Sinakevitch et al. 2008; Heinze and Reppert 2012). Most notably, across this order the lobes are considerably more complex than in most insects and consist of four parallel systems: the alpha/beta lobes, the alpha'/beta' lobes, the gamma lobes, and the Y-tract with its associated lobelets. While we identified all of these in the Bogong moth, the reliable separation of beta/beta' and alpha/alpha' lobes was not possible without

detailed examination of Kenyon cell projection patterns.

The lepidopteran calyx generally consists of an olfactory outer and a non-olfactory, often visual inner region (Stöckl et al. 2016; Sjöholm et al. 2005; Homberg et al. 1988; Kinoshita et al. 2015). Whereas the sensory inputs are not clear for the Monarch butterfly, the outer and inner zones of the calyx are also preserved in this species (Heinze & Reppert, 2012). Additionally, a third calyx compartment was distinguished, the basal zone, giving the calyx of the Monarch butterfly a more complex, almost bee-like appearance (Heinze & Reppert, 2012). The calyx of the Bogong moth follows the general moth layout with inner and outer ring, with the outer ring supplied via olfactory projections and the inner ring via optic lobe neurons.

An additional neuropil, the accessory calyx, is also present in all lepidopterans investigated in sufficient detail (Homberg et al. 1988; Heinze and Reppert 2012; Stöckl et al. 2016; Sjöholm et al. 2005; Kinoshita et al. 2015). In the Bogong moth this region is less well defined than in butterflies. As in *Papilio* butterflies and hawkmoths, visual projection neurons from the optic lobes supply input to the accessory calyx in the Bogong moth (Kinoshita et al., 2015; A. Stöckl et al., 2016). Overall, visual and olfactory inputs are thus segregated within the calyx, with the inner ring of the calyx and the accessory calyx being supplied with visual input and the large outer ring supplied by olfactory inputs. Another sensory modality, gustatory input, is present in the accessory calyces of locusts (Homberg et al. 2004) and crickets (Frambach & Schürmann, 2004), the dorsal accessory calyx in flies (Kirkhart & Scott, 2015) as well as in specific regions of the calyx in bees (Schröter & Menzel, 2003). This therefore might also exist in the Bogong moth.

While the sensory input to the moth calyx is segregated, the different sensory modalities share downstream processing networks, both in the calyx (Balkenius et al. 2009) and in the Kenyon cell population of the peduncle (Vogt et al., 2014). These networks encode visual and olfactory memories and underlie learning of visual and olfactory cues (Vogt et al., 2014). They are therefore likely not related to compass-based navigation, but crucial for odour- and colour-based foraging.

Nevertheless, odour information is likely of key importance for Bogong moths to locate their aestivation caves – odours likely provide the signal that terminates the migration (Warrant et al. 2016; Dreyer et al., in preparation). This behaviour must be hardwired and cannot be based on learning, given that each moth performs the migratory journey only once. The innate attraction to these specific olfactory cues is potentially mediated by neurons in the lateral horn. In fruit flies, these cells are known to encode odour valence (Schultzhaus, Saleem, Iftikhar, & Carney, 2017; Strutz et al., 2014) and specifically underly innate attraction or aversion to behaviourally highly relevant odours (Jefferis et al., 2007). The Bogong moth lateral horn is therefore an interesting target region for physiological and genetic studies that aim at understanding the mechanisms underlying the final segment of their migration – the short distance search for their aestivation caves.

Conclusion

The Bogong moth is a fascinating example of a nocturnal long-distance migrating insect with a rich sensory ecology. The anatomical framework of the brain presented here will

allow us to delve deeper into the open questions regarding the moth's migration. Firstly, we have provided a basis for qualitative and volumetric comparison between the brains of Bogong moths in different migratory states, as well as for interspecific comparisons to migratory and non-migratory insects. Second, we can now target specific brain regions with electrophysiology or molecular methods in order to explore their role in encoding compass information and guiding migratory behaviour. Finally, anatomical data from identified neurons, obtained from dye injections in conjunction with electrophysiological recordings, can be analysed more extensively by registering the neurons' anatomies into our standard atlas and thereby delineating functional neural circuits. Thus, by enabling future functional studies to be embedded within a detailed anatomical framework, we facilitate insights into the compass network that guides migration, the potential mechanisms of how olfactory information is used to identify migration targets after long distance flights, and the neural circuits that underpin magnetosensation.

Acknowledgements

The authors are grateful to Ken Green, David Dreyer and Kristina Brauburger for help with moth collection and maintenance, and to Eva Landgren for assistance with histology. We thank Dr. Erich Buchner, University of Würzburg for providing the anti-Synapsin antibody. We also thank the staff of the HPC cluster MaRC2 at the University of Marburg for their support. This work was funded by the US Airforce Office of Scientific Research (grant number FA9550-14-1-0242) to SH and EW, and the European Research Council (ERC) under the European Union's Horizon 2020 research and innovation program (grant agreement no. 714599 to S.H., and grant agreement no. 741298 to E.W.).

References

Aso, Y., Sitaraman, D., Ichinose, T., Kaun, K. R., Vogt, K., Belliart-Guérin, G., … Rubin, G. M. (2014). Mushroom body output neurons encode valence and guide memory-based action selection in Drosophila. *ELife*, *3*(3), e04580. https://doi.org/10.7554/eLife.04580

Balkenius, A., Bisch-Knaden, S., & Hansson, B. (2009). Interaction of visual and odour cues in the mushroom body of the hawkmoth Manduca sexta. *Journal of Experimental Biology*, *212*(4), 535–541. https://doi.org/10.1242/jeb.021220

Berg, B. G., Almaas, T. J., Bjaalie, J. G., & Mustaparta, H. (1998). The macroglomerular complex of the antennal lobe in the tobacco budworm moth Heliothis virescens: Specified subdivision in four compartments according to information about biologically significant compounds. *Journal of Comparative Physiology - A Sensory, Neural, and Behavioral Physiology*, *183*(6), 669–682. https://doi.org/10.1007/s003590050290

Berg, Bente G., Galizia, C. G., Brandt, R., & Mustaparta, H. (2002). Digital atlases of the antennal lobe in two species of tobacco budworm moths, the oriental Helicoverpa assulta (male) and the American Heliothis virescens (male and female). *Journal of Comparative Neurology*, *446*(2), 123–134. https://doi.org/10.1002/cne.10180

Clarac, F., & Pearlstein, E. (2007). Invertebrate preparations and their contribution to neurobiology in the second half of the 20th century. *Brain Research Reviews*, *54*(1),

113–161. https://doi.org/10.1016/j.brainresrev.2006.12.007
Common, I. F. B. (1954). A study of the ecology of the adult Bogong moth, Agrotis infusa (Boisd.) (Lepidoptera: Noctuidae), with special reference to its behaviour during migration and aestivation. *Aust. J. Zool.*, *2*(2), 223–263.
Cronin, T. W., Warrant, E. J., & Greiner, B. (2006). Celestial polarization patterns during twilight. *Applied Optics*, *45*(22), 5582–5589. https://doi.org/10.1364/AO.45.005582
de Vries, L., Pfeiffer, K., Trebels, B., Adden, A. K., Green, K., Warrant, E., & Heinze, S. (2017). Comparison of navigation-related brain regions in migratory versus non-migratory noctuid moths. *Frontiers in Behavioural Neuroscience*, *11*. https://doi.org/doi: 10.3389/fnbeh.2017.00158
Dreyer, D., Frost, B., Mouritsen, H., Günther, A., Green, K., Whitehouse, M., … Warrant, E. (2018). The Earth's Magnetic Field and Visual Landmarks Steer Migratory Flight Behavior in the Nocturnal Australian Bogong Moth. *Current Biology*, *28*, 1–7.
Eaton, J. L., Tignor, K. R., & Holtzman, G. I. (1983). Role of moth ocelli in timing flight initiation at dusk. *Physiological Entomology*, *8*(4), 371–375. https://doi.org/10.1111/j.1365-3032.1983.tb00370.x
el Jundi, B., Baird, E., Byrne, M. J., & Dacke, M. (2019). The brain behind straight-line orientation in dung beetles. *Journal of Exp*, (222), 1–7. https://doi.org/10.1242/jeb.192450
el Jundi, B., Huetteroth, W., Kurylas, A. E., & Schachtner, J. (2009). Anisometric brain dimorphism revisited: Implementation of a volumetric 3D standard brain in Manduca sexta. *Journal of Comparative Neurology*, *517*(2), 210–225. https://doi.org/10.1002/cne.22150
Frambach, I., & Schürmann, F. W. (2004). Separate distribution of deutocerebral projection neurons in the mushroom bodies of the cricket brain. *Acta Biologica Hungarica*, *55*(1–4), 21–29. https://doi.org/10.1556/ABiol.55.2004.1-4.4
Green, J., Adachi, A., Shah, K. K., Hirokawa, J. D., Magani, P. S., & Maimon, G. (2017). A neural circuit architecture for angular integration in Drosophila. *Nature*, *546*(7656), 101–106. https://doi.org/10.1038/nature22343
Gronenberg, W. (2001). Subdivisions of hymenopteran mushroom body calyces by their afferent supply. *Journal of Comparative Neurology*, *435*(4), 474–489. https://doi.org/10.1002/cne.1045
Guerra, P. A., Gegear, R. J., & Reppert, S. M. (2014). A magnetic compass aids monarch butterfly migration. *Nature Communications*, *5*. https://doi.org/10.1038/ncomms5164
Hansson, B. S., Anton, S., & Christensen, T. A. (1994). Structure and function of antennal lobe neurons in the male turnip moth, Agrotis segetum (Lepidoptera: Noctuidae). *Journal of Comparative Physiology A*, *175*(5), 547–562. https://doi.org/10.1007/BF00199476
Heinze, S. (2014). Polarized Light and Polarization Vision in Animal Sciences. In G. Horváth (Ed.), *Polarized Light and Polarization Vision in Animal Sciences* (pp. 61–111). Springer-Verlag Berlin Heidelberg. https://doi.org/10.1007/978-3-642-54718-8
Heinze, S., Florman, J., Asokaraj, S., el Jundi, B., & Reppert, S. M. (2013). Anatomical basis of sun compass navigation II: The neuronal composition of the central complex of the

monarch butterfly. *Journal of Comparative Neurology*, *521*(2), 267–298. https://doi.org/10.1002/cne.23214

Heinze, S., & Homberg, U. (2008). Neuroarchitecture of the central complex of the desert locust: Intrinsic and columnar neurons. *Journal of Comparative Neurology*, *511*(4), 454–478. https://doi.org/10.1002/cne.21842

Heinze, S., & Reppert, S. M. (2011). Sun Compass Integration of Skylight Cues in Migratory Monarch Butterflies. *Neuron*, *69*(2), 345–358. https://doi.org/10.1016/j.neuron.2010.12.025

Heinze, S., & Reppert, S. M. (2012). Anatomical basis of sun compass navigation I: The general layout of the monarch butterfly brain. *Journal of Comparative Neurology*, *520*(8), 1599–1628. https://doi.org/10.1002/cne.23054

Homberg, U., Montague, R. A., & Hildebrand, J. G. (1988). Anatomy of antenno-cerebral pathways in the brain of the sphinx moth Manduca sexta. *Cell and Tissue Research*, *254*(2), 255–281. https://doi.org/10.1007/BF00225800

Homberg, Uwe. (2015). Sky Compass Orientation in Desert Locusts — Evidence from Field and Laboratory Studies. *Frontiers in Behavioral Neuroscience*, *9*. https://doi.org/10.3389/fnbeh.2015.00346

Homberg, Uwe, Brandl, C., Clynen, E., Schoofs, L., & Veenstra, J. A. (2004). Mas-allatotropin/Lom-AG-myotropin I immunostaining in the brain of the locust, Schistocerca gregaria. *Cell and Tissue Research*, *318*(2), 439–457. https://doi.org/10.1007/s00441-004-0913-7

Homberg, Uwe, Hofer, S., Pfeiffer, K., & Gebhardt, S. (2003). Organization and Neural Connections of the Anterior Optic Tubercle in the Brain of the Locust, Schistocerca gregaria. *The Journal of Comparative Neurology*, *462*(4), 415–430. https://doi.org/10.1002/cne.10771

Honkanen, A., Adden, A., da Silva Freitas, J., & Heinze, S. (2019). The insect central complex and the neural basis of navigational strategies. *Journal of Experimental Biology*, *222*. https://doi.org/10.1242/jeb.188854

Ian, E., Berg, A., Lillevoll, S. C., & Berg, B. G. (2016). Antennal-lobe tracts in the noctuid moth, Heliothis virescens: new anatomical findings. *Cell and Tissue Research*, *366*(1), 23–35. https://doi.org/10.1007/s00441-016-2448-0

Immonen, E. V., Dacke, M., Heinze, S., & el Jundi, B. (2017). Anatomical organization of the brain of a diurnal and a nocturnal dung beetle. *Journal of Comparative Neurology*, *525*(8), 1879–1908. https://doi.org/10.1002/cne.24169

Ito, K., Shinomiya, K., Ito, M., Armstrong, J. D., Boyan, G., Hartenstein, V., … Vosshall, L. B. (2014). A systematic nomenclature for the insect brain. *Neuron*, *81*(4), 755–765. https://doi.org/10.1016/j.neuron.2013.12.017

Iwano, M., Hill, E. S., Mori, A., Mishima, T., Mishima, T., Ito, K., & Kanzaki, R. (2010). Neurons Associated With the Flip-Flop Activity in the Lateral Accessory Lobe and Ventral Protocerebrum of the Silkworm Moth Brain. *The Journal of Comparative Neurology*, *518*(3), 366–388. https://doi.org/10.1002/cne.22224

Jarriault, D., Gadenne, C., Lucas, P., Rospars, J. P., & Anton, S. (2010). Transformation of the sex pheromone signal in the noctuid moth Agrotis ipsilon: From peripheral input to

antennal lobe output. *Chemical Senses*, *35*(8), 705–715. https://doi.org/10.1093/chemse/bjq069

Jefferis, G. S. X. E., Potter, C. J., Chan, A. M., Marin, E. C., Rohlfing, T., Maurer, C. R., & Luo, L. (2007). Comprehensive Maps of Drosophila Higher Olfactory Centers: Spatially Segregated Fruit and Pheromone Representation. *Cell*, *128*(6), 1187–1203. https://doi.org/10.1016/j.cell.2007.01.040

Jenett, A., Rubin, G. M., Ngo, T. T. B., Shepherd, D., Murphy, C., Dionne, H., … Zugates, C. T. (2012). A GAL4-Driver Line Resource for Drosophila Neurobiology. *Cell Reports*, *2*(4), 991–1001. https://doi.org/10.1016/j.celrep.2012.09.011

Kazawa, T., Namiki, S., Fukushima, R., Terada, M., Soo, K., & Kanzaki, R. (2009). Constancy and variability of glomerular organization in the antennal lobe of the silkmoth. *Cell and Tissue Research*, *336*(1), 119–136. https://doi.org/10.1007/s00441-009-0756-3

King, J. R., Christensen, T. A., & Hildebrand, J. G. (2000). Response characteristics of an identified, sexually dimorphic olfactory glomerulus. *Journal of Neuroscience*, *20*(6), 2391–2399.

Kinoshita, M., Shimohigasshi, M., Tominaga, Y., Arikawa, K., & Homberg, U. (2015). Topographically distinct visual and olfactory inputs to the mushroom body in the swallowtail butterfly, papilio xuthus. *Journal of Comparative Neurology*, *523*(1), 162–182. https://doi.org/10.1002/cne.23674

Kirkhart, C., & Scott, K. (2015). Gustatory learning and processing in the Drosophila mushroom bodies. *Journal of Neuroscience*, *35*(15), 5950–5958. https://doi.org/10.1523/JNEUROSCI.3930-14.2015

Klagges, B. R. E., Heimbeck, G., Godenschwege, T. A., Hofbauer, A., Pflugfelder, G. O., Reifegerste, R., … Buchner, E. (1996). Invertebrate Synapsins: A Single Gene Codes for Several Isoforms in Drosophila. *The Journal of Neuroscience*, *16*(10), 3154–3165.

Kvello, P., Løfaldli, B. B., Rybak, J., Menzel, R., & Mustaparta, H. (2009). Digital, three-dimensional average shaped atlas of the Heliothis virescens brain with integrated gustatory and olfactory neurons. *Frontiers in Systems Neuroscience*, *3*(OCT), 1–14. https://doi.org/10.3389/neuro.06.014.2009

Lin, C., & Strausfeld, N. J. (2012). Visual inputs to the mushroom body calyces of the whirligig beetle Dineutus sublineatus: Modality switching in an insect. *Journal of Comparative Neurology*, *520*(12), 2562–2574. https://doi.org/10.1002/cne.23092

Menzel, R. (2014). The insect mushroom body, an experience-dependent recoding device. *Journal of Physiology Paris*, *108*(2–3), 84–95. https://doi.org/10.1016/j.jphysparis.2014.07.004

Montgomery, S. H., Merrill, R. M., & Ott, S. R. (2016). Brain composition in Heliconius butterflies, posteclosion growth and experience-dependent neuropil plasticity. *Journal of Comparative Neurology*, *524*(9), 1747–1769. https://doi.org/10.1002/cne.23993

Mota, T., Yamagata, N., Giurfa, M., Gronenberg, W., & Sandoz, J.-C. (2011). Neural Organization and Visual Processing in the Anterior Optic Tubercle of the Honeybee Brain. *Journal of Neuroscience*, *31*(32), 11443–11456. https://doi.org/10.1523/JNEUROSCI.0995-11.2011

Mouritsen, H., Derbyshire, R., Stalleicken, J., Mouritsen, O. Ø., Frost, B. J., & Norris, D. R. (2013). An experimental displacement and over 50 years of tag-recoveries show that monarch butterflies are not true navigators. *PNAS*, *110*(18), 7348–7353. https://doi.org/10.1073/pnas.1221701110/-/DCSupplemental.www.pnas.org/cgi/doi/10.1073/pnas.1221701110

Namiki, S., & Kanzaki, R. (2016). Neurobiological basis of orientation behavior in insects: Insights from the silkmoth mating dance. *Current Opinion in Insect Science*, *in press*(February). https://doi.org/10.1016/j.cois.2016.02.009

Omoto, J. J., Keleş, M. F., Nguyen, B. C. M., Bolanos, C., Lovick, J. K., Frye, M. A., & Hartenstein, V. (2017). Visual Input to the Drosophila Central Complex by Developmentally and Functionally Distinct Neuronal Populations. *Current Biology*, *27*(8), 1098–1110. https://doi.org/10.1016/j.cub.2017.02.063

Ott, S. R. (2008). Confocal microscopy in large insect brains: Zinc-formaldehyde fixation improves synapsin immunostaining and preservation of morphology in whole-mounts. *Journal of Neuroscience Methods*, *172*, 220–230. https://doi.org/10.1016/j.jneumeth.2008.04.031

Paulk, A. C., & Gronenberg, W. (2008). Higher order visual input to the mushroom bodies in the bee, Bombus impatiens. *Arthropod Structure and Development*, *37*(6), 443–458. https://doi.org/10.1016/j.asd.2008.03.002

Pfeiffer, K., & Homberg, U. (2007). Coding of Azimuthal Directions via Time-Compensated Combination of Celestial Compass Cues. *Current Biology*, *17*(11), 960–965. https://doi.org/10.1016/j.cub.2007.04.059

Pfeiffer, K., Kinoshita, M., & Homberg, U. (2005). Polarization-sensitive and light-sensitive neurons in two parallel pathways passing through the anterior optic tubercle in the locust brain. *Journal of Neurophysiology*, *94*(6), 3903–3915. https://doi.org/10.1152/jn.00276.2005

Preibisch, S., Saalfeld, S., & Tomancak, P. (2009). Globally optimal stitching of tiled 3D microscopic image acquisitions. *Bioinformatics*, *25*(11), 1463–1465. https://doi.org/10.1093/bioinformatics/btp184

Reppert, S. M., Guerra, P. A., & Merlin, C. (2016). Neurobiology of Monarch Butterfly Migration. *Annual Review of Entomology*, *61*(1), 25–42. https://doi.org/10.1146/annurev-ento-010814-020855

Ritz, T., Adem, S., & Schulten, K. (2000). A Model for Photoreceptor-Based Magnetoreception in Birds. *Biophysical Journal*, *78*(2), 707–718. https://doi.org/10.1016/S0006-3495(00)76629-X

Rohlfing, T., Brandt, R., Maurer, C. R., & Menzel, R. (2001). Bee brains, B-splines and computational democracy: Generating an average shape atlas. *Proceedings of the Workshop on Mathematical Methods in Biomedical Image Analysis*, 187–194.

Rohlfing, T., & Maurer, C. R. (2007). Shape-Based Averaging. *IEEE Transactions on Image Processing*, *16*(1), 153–161.

Schindelin, J., Arganda-Carreras, I., Frise, E., Kaynig, V., Longair, M., Pietzsch, T., … Cardona, A. (2012). Fiji: An open-source platform for biological-image analysis. *Nature Methods*, *9*(7), 676–682. https://doi.org/10.1038/nmeth.2019

Schröter, U., & Menzel, R. (2003). A new ascending sensory tract to the calyces of the honeybee mushroom body, the subesophageal-calycal tract. *Journal of Comparative Neurology*, *465*(2), 168–178. https://doi.org/10.1002/cne.10843

Schulten, K., Swenberg, C. E., & Weiler, A. (1978). A Biomagnetic Sensory Mechanism Based on Magnetic Field Modulated Coherent Electron Spin Motion. *Zeitschrift Fur Physikalische Chemie*, *111*(1), 1–5. https://doi.org/10.1524/zpch.1978.111.1.001

Schultzhaus, J. N., Saleem, S., Iftikhar, H., & Carney, G. E. (2017). The role of the Drosophila lateral horn in olfactory information processing and behavioral response. *Journal of Insect Physiology*, *98*, 29–37. https://doi.org/10.1016/j.jinsphys.2016.11.007

Seelig, J. D., & Jayaraman, V. (2013). Feature detection and orientation tuning in the Drosophila central complex. *Nature*, *503*(7475), 262. https://doi.org/10.1038/nature12601

Shiozaki, H. M., & Kazama, H. (2017). Parallel encoding of recent visual experience and self-motion during navigation in Drosophila. *Nature Neuroscience*, *20*(10), 1395–1403. https://doi.org/10.1038/nn.4628

Sinakevitch, I., Sjöholm, M., Hansson, B. S., & Strausfeld, N. J. (2008). Global and local modulatory supply to the mushroom bodies of the moth Spodoptera littoralis. *Arthropod Structure and Development*, *37*(4), 260–272. https://doi.org/10.1016/j.asd.2008.01.001

Sjöholm, M., Sinakevitch, I., Ignell, R., Strausfeld, N. J., & Hansson, B. S. (2005). Organization of Kenyon cells in subdivisions of the mushroom bodies of a lepidopteran insect. *Journal of Comparative Neurology*, *491*(3), 290–304. https://doi.org/10.1002/cne.20698

Skiri, H. T., Rø, H., Berg, B. G., & Mustaparta, H. (2005). Consistent organization of glomeruli in the antennal lobes of related species of heliothine moths. *Journal of Comparative Neurology*, *491*(4), 367–380. https://doi.org/10.1002/cne.20692

Stange, G. (1981). The ocellar component of flight equilibrium control in dragonflies. *Journal of Comparative Physiology □ A*, *141*(3), 335–347. https://doi.org/10.1007/BF00609936

Stöckl, A., Heinze, S., Charalabidis, A., el Jundi, B., Warrant, E., & Kelber, A. (2016). Differential investment in visual and olfactory brain areas reflects behavioural choices in hawk moths. *Scientific Reports*, (6), 1–10. https://doi.org/10.1038/srep26041

Stöckl, A. L., & Heinze, S. (2015). A clearer view of the insect brain — combining bleaching with standard whole-mount immunocytochemistry allows confocal imaging of pigment-covered brain areas for 3D reconstruction. *Frontiers in Neuroanatomy*, *9*(September), 1–8. https://doi.org/10.3389/fnana.2015.00121

Stone, T., Webb, B., Adden, A., Weddig, N. Ben, Honkanen, A., Templin, R., … Heinze, S. (2017). An Anatomically Constrained Model for Path Integration in the Bee Brain. *Current Biology*, *27*(20), 3069-3085.e11. https://doi.org/10.1016/j.cub.2017.08.052

Strausfeld, Nicholas J., Hansen, L., Li, Y., Gomez, R. S., & Ito, K. (1998). Evolution, discovery, and interpretations of arthropod mushroom bodies. *Learning and Memory*, *5*(1–2), 11–37.

Strausfeld, Nicholas J., Sinakevitch, I., Brown, S. M., & Farris, S. M. (2009). Ground plan of the insect mushroom body: Functional and evolutionary implications. *Journal of*

Comparative Neurology, *513*(3), 265–291. https://doi.org/10.1002/cne.21948
Strausfeld, Nicolas J. (2012). *Arthropod Brains*. Cambridge, Massachusetts, London, England: Harvard University Press.
Strube-Bloss, M. F., Nawrot, M. P., & Menzel, R. (2011). Mushroom body output neurons encode odor-reward associations. *Journal of Neuroscience*, *31*(8), 3129–3140. https://doi.org/10.1523/JNEUROSCI.2583-10.2011
Strutz, A., Soelter, J., Baschwitz, A., Farhan, A., Grabe, V., Rybak, J., … Sachse, S. (2014). Decoding odor quality and intensity in the Drosophila brain. *ELife*, *3*, e04147. https://doi.org/10.7554/eLife.04147
Turner-Evans, D., Wegener, S., Rouault, H., Franconville, R., Wolff, T., Seelig, J. D., … Jayaraman, V. (2017). Angular velocity integration in a fly heading circuit. *ELIFE*, *6*, e23496. https://doi.org/10.7554/eLife.23496
Varga, A. G., & Ritzmann, R. E. (2016). Cellular Basis of Head Direction and Contextual Cues in the Insect Brain. *Current Biology*, *26*(14), 1816–1828. https://doi.org/10.1016/j.cub.2016.05.037
Vogt, K., Schnaitmann, C., Dylla, K. V., Knapek, S., Aso, Y., Rubin, G. M., & Tanimoto, H. (2014). Shared mushroom body circuits underlie visual and olfactory memories in Drosophila. *ELife*, *3*, e02395. https://doi.org/10.7554/eLife.02395
von Hadeln, J., Althaus, V., Häger, L., & Homberg, U. (2018). Anatomical organization of the cerebrum of the desert locust Schistocerca gregaria. *Cell and Tissue Research*, *374*(1), 39–62. https://doi.org/10.1007/s00441-018-2844-8
Warrant, E., Frost, B., Green, K., Mouritsen, H., Dreyer, D., Adden, A., … Heinze, S. (2016). The australian bogong moth Agrotis infusa: A long-distance nocturnal navigator. *Frontiers in Behavioral Neuroscience*, *10*(April). https://doi.org/10.3389/fnbeh.2016.00077
Warrant, Eric, & Dacke, M. (2016). Visual Navigation in Nocturnal Insects. *Physiology*, *31*(4), 182–192. https://doi.org/10.1152/physiol.00046.2015
Williams, J. L. D. (1975). Anatomical studies of the insect central nervous system: A ground-plan of the midbrain and an introduction to the central complex in the locust, Schistocerca gregaria (Orthoptera). *Journal of Zoology*, *176*(1), 67–86. https://doi.org/10.1111/j.1469-7998.1975.tb03188.x
Wolff, T., Iyer, N. A., & Rubin, G. M. (2015). Neuroarchitecture and neuroanatomy of the Drosophila central complex: A GAL4-based dissection of protocerebral bridge neurons and circuits. *Journal of Comparative Neurology*, *523*(7), 997–1037. https://doi.org/10.1002/cne.23705
Wunderer, H., & de Kramer, J. J. (1989). Dorsal ocelli and light-induced diurnal activity patterns in the arctiid moth Creatonotos transiens. *Journal of Insect Physiology*, *35*(2), 87–95. https://doi.org/10.1016/0022-1910(89)90041-3
Zeil, J., Ribi, W. A., & Narendra, A. (2014). Polarisation Vision in Ants, Bees and Wasps. In G. Horváth (Ed.), *Polarized Light and Polarization Vision in Animal Sciences* (pp. 41–60). Berlin, Heidelberg: Springer.
Zeller, M., Held, M., Bender, J., Berz, A., Heinloth, T., Hellfritz, T., & Pfeiffer, K. (2015). Transmedulla Neurons in the Sky Compass Network of the Honeybee (Apis mellifera)

Are a Possible Site of Circadian Input. *PLoS ONE*, *10*(12), 1–25. https://doi.org/10.1371/journal.pone.0143244

Zorovic, M., & Hedwig, B. (2011). Processing of species-specific auditory patterns in the cricket brain by ascending, local, and descending neurons during standing and walking. *Journal of Neurophysiology*, *105*(5), 2181–2194. https://doi.org/10.1152/jn.00416.2010

Insect brain database. Agrotis infusa 3D atlas available at https://hdl.handle.net/20.500.12158/SIN-0000002.1

TABLE 2 Mean absolute volumes of male and female Bogong moth brains and neuropils.

Neuropil	Male brain – absolute volume (μm^3)	Male brain – SD (μm^3)	Female brain – absolute volume (μm^3)	Female brain – SD (μm^3)
PC	**9.55×10^7**	**1.94×10^7**	**7.88×10^7**	**2.75×10^5**
OL	**5.63×10^7**	**9.24×10^6**	**5.42×10^7**	**6.04×10^6**
ME	4.20×10^7	7.10×10^6	4.01×10^7	4.87×10^6
LO	9.80×10^6	1.56×10^6	9.23×10^6	8.66×10^5
LOP	4.27×10^6	7.33×10^5	4.52×10^6	2.66×10^5
AME	2.61×10^5	5.91×10^4	3.09×10^5	4.24×10^4
AL	**2.13×10^7**	**4.64×10^6**	**1.55×10^7**	**1.01×10^6**
MB	**8.26×10^6**	**1.97×10^6**	**7.05×10^6**	**1.13×10^4**
CA	4.95×10^6	1.35×10^6	4.55×10^6	2.47×10^5
PED	5.59×10^5	1.66×10^5	5.14×10^5	5.37×10^4
Lobes	2.75×10^6	5.16×10^5	1.99×10^6	2.89×10^5
alpha/alpha'	*3.05×10^5*	*9.14×10^4*	*2.11×10^5*	*2.62×10^4*
beta/beta'	*8.58×10^5*	*1.52×10^5*	*5.46×10^5*	*1.48×10^5*
medial gamma	*4.54×10^5*	*9.80×10^4*	*4.09×10^5*	*1.39×10^5*
vertical gamma	*1.98×10^5*	*6.29×10^4*	*1.49×10^5*	*1.98×10^4*
spur	*1.99×10^5*	*4.71×10^4*	*1.57×10^5*	*3.54×10^3*
Y	*7.37×10^5*	*1.07×10^5*	*5.15×10^5*	*1.27×10^4*
LX	**3.65×10^6**	**6.26×10^5**	**3.55×10^6**	**1.80×10^5**
LAL	3.56×10^6	6.02×10^5	3.46×10^6	1.80×10^5
BU	5.14×10^4	1.34×10^4	6.35×10^4	3.54×10^3
GA	4.74×10^4	2.64×10^4	3.20×10^4	4.24×10^3
CX	**2.27×10^6**	**2.89×10^5**	**1.90×10^6**	**5.66×10^3**
FB	1.58×10^6	2.02×10^5	1.30×10^6	3.25×10^4
EB	4.27×10^5	7.16×10^4	3.27×10^5	7.07×10^2
PB	1.91×10^5	4.35×10^4	1.89×10^5	4.95×10^3
NO	7.63×10^4	1.93×10^4	8.45×10^4	4.17×10^4
AOTU	**9.81×10^5**	**1.78×10^5**	**8.73×10^5**	**1.13×10^5**
UU	7.91×10^5	1.24×10^5	6.69×10^5	7.57×10^4
LU	6.52×10^4	2.25×10^4	6.70×10^4	2.83×10^3
NU	1.25×10^5	3.53×10^4	1.37×10^5	3.54×10^4
ONP	**2.14×10^5**	**7.17×10^4**	**2.41×10^5**	**1.52×10^5**
Whole brain	**1.88×10^8**	**3.51×10^7**	**1.62×10^8**	**4.82×10^6**

TABLE 3 Mean relative volumes of the neuropils of six male and two female Bogong moth brains. The normalised standard deviation (SD) is the percentage by which the volume varies around the mean (absolute SD / absolute mean x 100).

Neuropil	Male brain – relative volume (%)	Male brain – normalised SD (%)	Female brain – relative volume (%)	Female brain – normalised SD (%)
PC	**50.51**	**20.30**	**48.65**	**0.35**
OL	**30.01**	**16.42**	**33.40**	**11.14**
ME	22.36	16.92	24.73	12.12
LO	5.24	15.91	5.69	9.39
LOP	2.27	17.17	2.79	5.88
AME	0.14	22.64	0.19	13.73
AL	**11.28**	**21.72**	**9.55**	**6.56**
MB	**4.36**	**23.89**	**4.35**	**0.16**
CA	2.60	27.39	2.81	5.44
PED	0.29	29.65	0.32	10.46
Lobes	1.47	18.76	1.22	14.57
alpha/alpha'	*0.16*	*30.00*	*0.13*	*12.43*
beta/beta'	*0.46*	*17.75*	*0.34*	*27.09*
Medial gamma	*0.24*	*21.62*	*0.25*	*33.89*
Vertical gamma	*0.10*	*31.76*	*0.09*	*13.29*
Spur	*0.11*	*23.69*	*0.10*	*2.26*
Y	*0.40*	*14.49*	*0.32*	*2.47*
LX	**1.97**	**17.13**	**2.19**	**5.06**
LAL	1.92	16.94	2.13	5.20
BU	0.03	26.00	0.04	5.57
GA	0.02	55.71	0.02	13.26
CX	**1.22**	**12.70**	**1.17**	**0.30**
FB	0.85	12.77	0.80	2.51
EB	0.23	16.75	0.20	0.22
PB	0.10	22.85	0.12	2.63
NO	0.04	25.29	0.05	49.37
AOTU	**0.53**	**18.18**	**0.54**	**12.96**
UU	0.42	15.72	0.41	11.32
LU	0.03	34.52	0.04	4.22
NU	0.07	28.13	0.08	25.81
ONP	**0.11**	**33.51**	**0.15**	**63.21**